ABSTRACT

Title of Thesis: ADVANCED SULFIDE SOLID ELECTROLYTE ENABLED BY NITROGEN DOPING

Xiangyang Zhu, Master of Science, 2017

Thesis Directed By: Professor Chunsheng Wang, Department of Chemical and Biomolecular Engineering

All-solid-state lithium batteries (ASSLBs) are being considered as the ultimate solution to the safety issue of current lithium ion batteries which use flammable organic electrolyte. The properties of the solid electrolyte, the most important component in ASSLBs, largely affect the electrode/electrolyte interfacial behavior and eventually the performance of ASSLBs. Sulfide electrolytes are considered as one of the most promising solid electrolyte for ASSLBs because of its excellent mechanical properties. However, they suffer from poor electrochemical stability and lithium dendrite formation. In this thesis, I demonstrated that the nitrogen-doped sulfide solid electrolyte system $(75\text{-}1.5x)Li_2S\text{-}25P_2S_5\text{-}xLi_3N$ showed comprehensive performance improvements. The ionic conductivity is enhanced and the interfacial resistance between Li anode and solid electrolyte gets reduced by over 80%. The dendrite formation in solid electrolyte could also be effectively suppressed with the critical current density enhanced by 70%. The simultaneous improvement make it a promising solid electrolyte for ASSLBs.

ADVANCED SULFIDE SOLID ELECTROLYTE ENABLED BY NITROGEN DOPING

by

Xiangyang Zhu

Thesis submitted to the Faculty of the Graduate School of the
University of Maryland, College Park, in partial fulfillment
of the requirements for the degree of
Master of Science
2017

Advisory Committee:
Professor Chunsheng Wang, Chair
Professor Nam Sun Wang
Professor Taylor J. Woehl

Acknowledgements

I would first like to express my sincere gratitude to my thesis advisor Prof. Chunsheng Wang for his encouragement, guidance and support throughout my whole research study.

I would also like to thank my colleagues, Mr. Fudong Han and Ms. Jie Yue. We have plenty of discussions which is really helpful to optimize my experiment design. Besides, Mr. Fudong Han also helped me with the XRD and SEM test. Without their passionate participation and input, the experiment could not have been successfully conducted.

At last, I would like to thank my families. Without their support, I could not have the chance to continue my graduate study.

Table of Contents

List of Tables

List of Figures

Chapter 1: Introduction

1.1 Demand for Renewable Energy Source

Nowadays the energy economy is more and more relied on fossil fuel in daily lives. The demand for fossil fuel has been increasing year after year, but it is a kind of non-renewable source. The shortage of fossil fuel will be a very serious problem in the near future. The consumption of fossil fuel also causes environmental problem like greenhouse effect due to the emission of huge plenty of carbon dioxide during the burning of fossil fuel. In order to solve the problems of energy supply and environmental pollution, it is necessary to seek a new kind of renewable and environmentally-friendly energy source to replace the traditional fossil fuel. Different kinds of renewable energy have been developed in past several decades, i.e. electrical energy, solar energy, nuclear energy, biofuel and so on. Among the various kinds of new energy, electrical energy is the most convenient form since it is easy and efficient to store and distribute. Thus the energy storage system based on electrochemical energy has been developed and applied in electric vehicles(EVs), hybrid electric vehicles(HEVs) and plug-in electric vehicles(PHEVs) [1]. The appearance of EVs not only meets the renewable energy requirements but also solves the environmental issues with zero emission of carbon dioxide. One major challenge for EVs is developing the power and energy density of electrochemical storage systems. Hundreds of different battery technologies have been proposed since nineteenth century. The most common secondary batteries are designed based on lead-acid, Ni-Cd, Ni-MH and lithium ion technologies [2]. Among these different

kinds of batteries, lithium ion battery (LIB) has advantages of higher volumetric and gravimetric energy density corresponding to smaller size and lighter weight (Fig. 1.1).

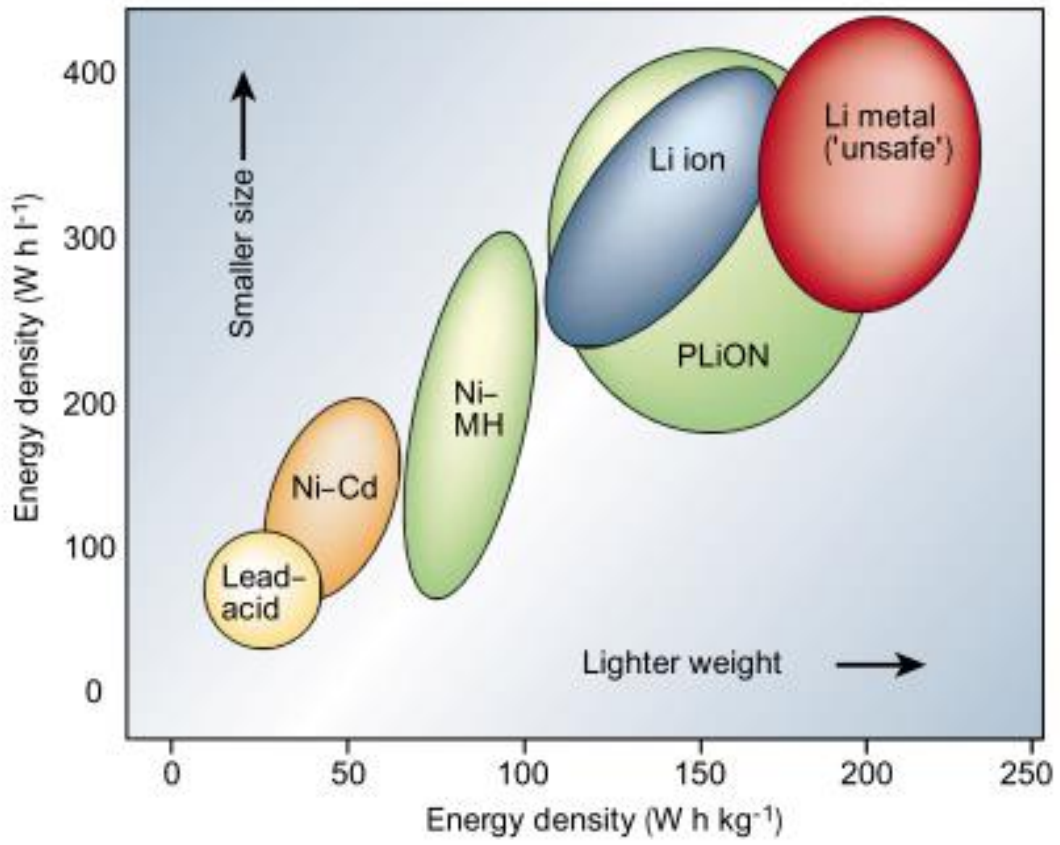

Figure 1.1. Comparison of the different battery technologies based on the volumetric and gravimetric energy density [2]

The first commercialized LIB was appeared in 1991 by SONY via exchanging the lithium ion between graphite anode and a layered-oxide cathode. Billions of LIBs have been produced for portable electronic devices since then [3]. However, the power and energy density of current commercial LIBs are still not high enough to meet the requirement for transport applications. Tremendous research effort is devoted to solving such kind of problem. Besides, the lithium metal rechargeable

battery is also under development in order to achieve the request of high energy density.

1.2 Basic Principle of Lithium Ion Battery System

1.2.1 Operating Principle of LIB System

A common LIB consists of three parts: anode, cathode and electrolyte. The lithium ions are transported between the anode and cathode during charge and discharge process (Fig. 1.2). Figure 1.2 provides an example of operating mechanism for a LIB consisting of graphite as the anode and $LiCoO_2$ as the cathode [4]. During

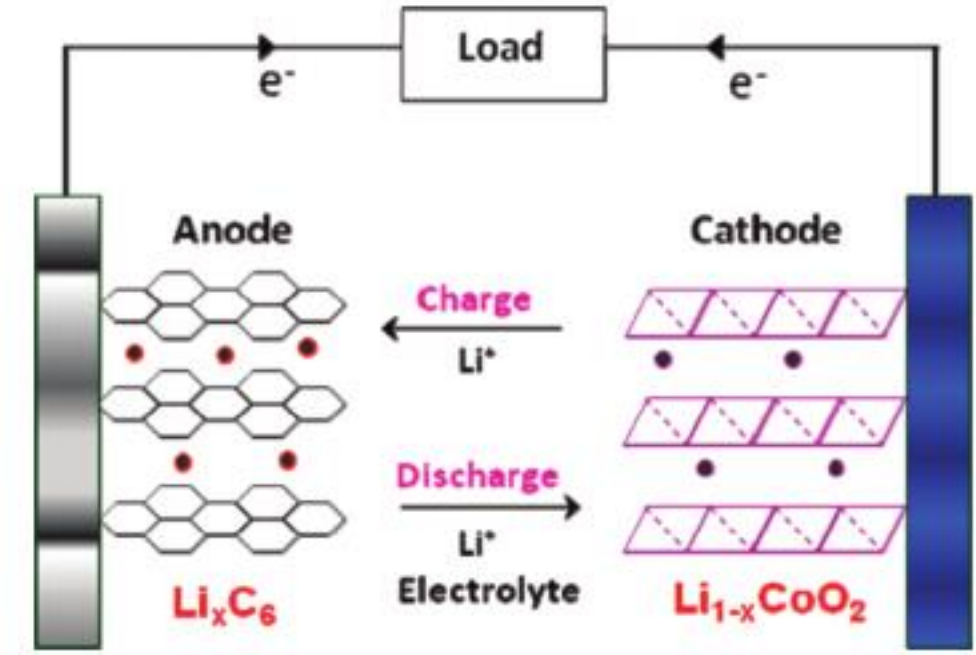

Figure 1.2. Schematic diagram of operating mechanism for a LIB with graphite as the anode and layered $LiCoO_2$ as the cathode [4].

the charge process, lithium ions come out from the cathode, transport through the electrolyte and insert into the anode. In the meantime, electrons drift from cathode to

anode by the external circuit due to the high ionic conductivity and low electronic conductivity of electrolyte. At the anode, lithium ions combine with electron to form lithium atoms and balance the charge. The discharge process is just the reverse of charge process. Lithium ions and electrons transport opposite direction and gather at the cathode. In order to prevent short-circuiting, separator is needed in electrolyte to prevent the direct contact between cathode and anode.

1.2.2 Materials for Cathode and Anode

The choice of electrodes and electrolyte materials determines a battery's' voltage and capacity which are directly related to its energy density. Based on structure types, the cathode materials can be categorized as three main types: layered structure, spinel and olivine. The anode materials can be categorized based on reaction types with lithium ion: intercalation/insertion reaction, alloying reaction and conversion reaction. The specific capacity of electrode material can be calculated from the equation:

$$Q_{(mAh/g)} = \frac{n(mol) * F(C/mol)}{W_{electrode}(g/mol) * 1mol} * 3.7(mAh/C)$$

where n stands for the amount of lithium ion that can be inserted into or extracted from the electrode. ; F is the Faradic constant which is equal to 26800 Coulomb per mole; $W_{electrode}$ represents the molecular weight of electrode; 3.7 is a factor converting the unit from coulomb to mAh.

The specific capacity of different materials for cathode or anode can be quantified and compared with the help of the above equation. The voltage and specific capacity of some common electrode materials have been shown in Figure 1.3

(Fig. 1.3). LiC_OO_2 [5], a kind of layered-structure cathode material, has specific capacity around 295 mAh/g. It has been widely used in portable devices like cell phones, laptops and cameras. The specific capacity of $LiMn_2O_4$ spinel [6] is around 150 mAh/g while that of $LiFePO_4$ olivine [7] is about 170 mAh/g. With a desire to

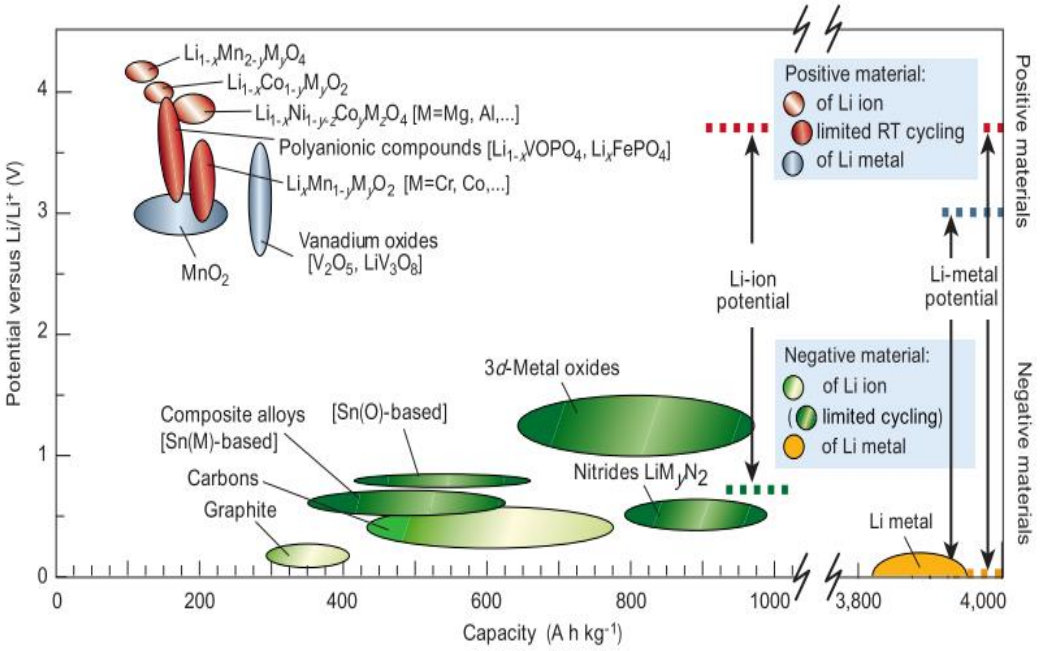

Figure 1.3. Potential versus capacity of some cathode and anode materials currently used or under considerations for next generation of LIBs [2].

increase the energy density, lots of research groups are focusing on discovering new cathode materials with high voltage and/or high specific capacity. The currently used anode materials for commercialized LIBs are mainly graphite with a specific capacity around 372 mAh/g [8]. Its reaction mechanism of inserting/extracting lithium ions is based on intercalation. Anode materials which can electrochemically alloy with lithium ions are able to provide much higher specific capacity. For instance, tin can alloy with lithium ion to form $Li_{4.4}Sn$ [9] providing a specific capacity of 993 mAh/g

and silicon can form $Li_{3.75}Si$ [10] alloy with a specific capacity as much as 3578 mAh/g. Transition metal oxide anodes, MO_x (M = Mo, Fe, Ni, etc…), could achieve reversible lithium ion storage through conversion reaction. MoO_3 anode accommodates lithium ions to form Li_xMoO_2 ($0<x<1$) with a theoretical specific capacity of 209mAh/g [11]. The total capacity of anode should match with that of cathode for a LIB to work.

1.2.3 Electrolyte and Solid Electrolyte Interphase

Electrolyte plays important role in LIB system by keeping the positive and negative electrodes apart to prevent electrical short and allowing only ionic charges to transport. Thus, electrolyte is required to have high lithium ion conductivity ($>10^{-4}$) and low electronic conductivity ($<10^{-10}$) [12]. Most lithium electrolytes are made by dissolving one or more lithium salts in mixtures of two or more solvents. In order to perform various functions simultaneously, solvents with different physical and chemical natures are usually used together. An ideal kind of lithium salt should be able to dissolve and disperse in the electrolyte solvent completely with high mobility of solvated ions [13]. Each kind of electrolyte has its own potential window. Electrodes will be stable with the electrolyte if their potential is within the window of electrolyte. Otherwise, an interface layer will be formed between the electrode and electrolyte. Such passivation film is formed due to the oxidation of electrolyte at high potential and the reduction of electrolyte at low potential. The electrolyte of 1 M LiPF6 dissolved in EC/DEC with a ratio of 1:1 is commonly used for LIB. As is shown in figure 1.4, the potential of most cathode materials lays inside its potential

window (Fig. 1.4). However, the potential of graphite anode does not reach the lower limit of the electrolyte's window. As a consequence, a surface film is formed due to

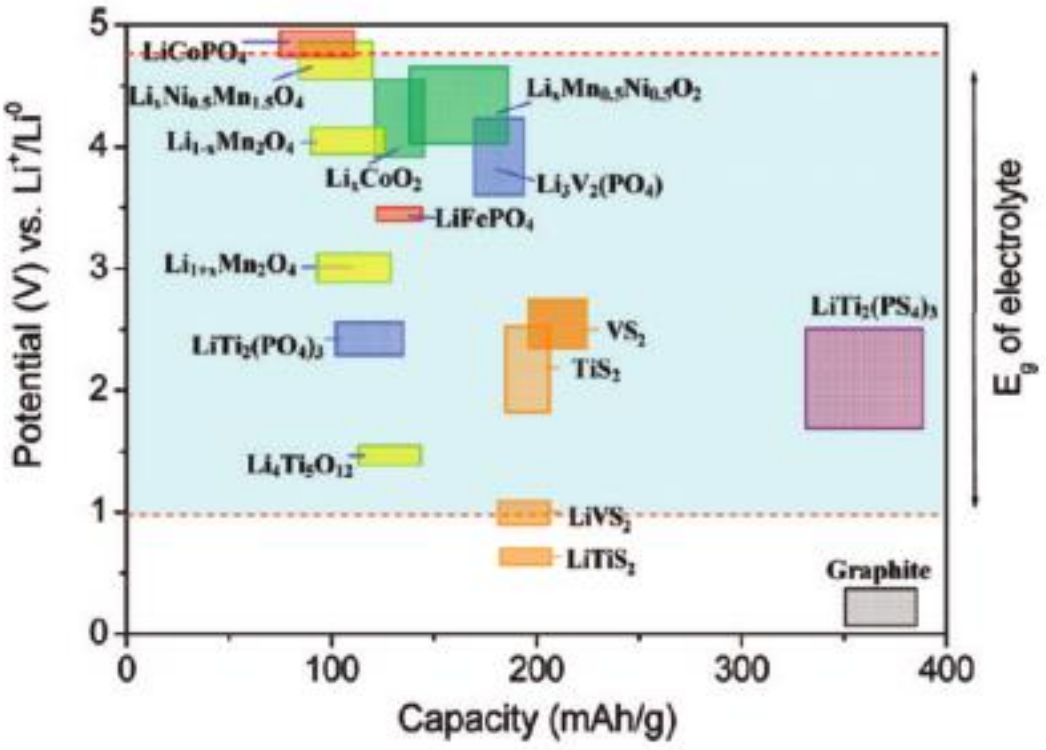

Figure 1.4. The potential window of the electrolyte 1 M LiPF6 in EC/DEC (1:1) with respect to several electrode materials [12].

the decomposition of electrolyte solvents. Dahn *et al.* named such surface film on carbonaceous anodes a "solid electrolyte interface" (SEI) [14]. The formation of a SEI layer consumes some amount of lithium ions which causes irreversible specific charge. This SEI layer is an ionic conductor but an electronic insulator. It can prevent further decomposition of the electrolyte components to stabilize reversible lithium insertion and extraction.

1.2.4 Challenges of Current LIBs

The demand for higher stored volumetric and gravimetric energy density of a LIB is continuously rising with the growing of electric automotive transportation and renewable energy storage markets. However, the capacities of cathode materials are hard to be enhanced at current stage. Thus, scientists are attempting to find new cathode materials with high voltage to enhance the energy density. Although silicon and tin are considered to be promising candidates for anode materials due to their high capacity, their large volume expansion (~300%) results in the electrode structure collapse and fast capacity decay. Both cations and anions of lithium salt in electrolyte can carry current, but only lithium ions matters for LIBs. The proportion of lithium ions is only around 0.2 to 0.4 for common electrolyte compositions. The temperature range of electrolyte is narrow. Commercialized LIBs can only deliver their rated capacity and the power in the range from -20 to 50 ^{o}C [13]. Liquid electrolyte is easy to catch fire and cause explosion when the battery short circuit happens. Besides, cost, discharge/charge rate and cycle life are also issues that hinder the development of LIBs.

1.3 All-Solid-State Lithium Battery (ASSLB)

1.3.1 Structure of ASSLBs

In order to solve the aforementioned challenges, several new battery technologies have arisen. Among these new technologies, all-solid-state lithium batteries (ASSLBs) are considered to be a potential candidate material for next-generation battery. Overcharging or short-circuiting can result in fires or explosions

during due to the flammability of organic electrolyte [15]. ASSLBs using inorganic solid electrolyte are considered to be an effective alternative to ultimately solve these safety issues [16]. The broad operating temperature is another important characterization for ASSLBs [17]. The structure of ASSLBs is similar as the traditional LIBs which are composed of anode, cathode and electrolyte (Fig.1.5). The working principle of ASSLBs is no different from the LIBs as described in section 1.2.1. Solid electrolyte can also serve as separator due to its mechanical property [18].

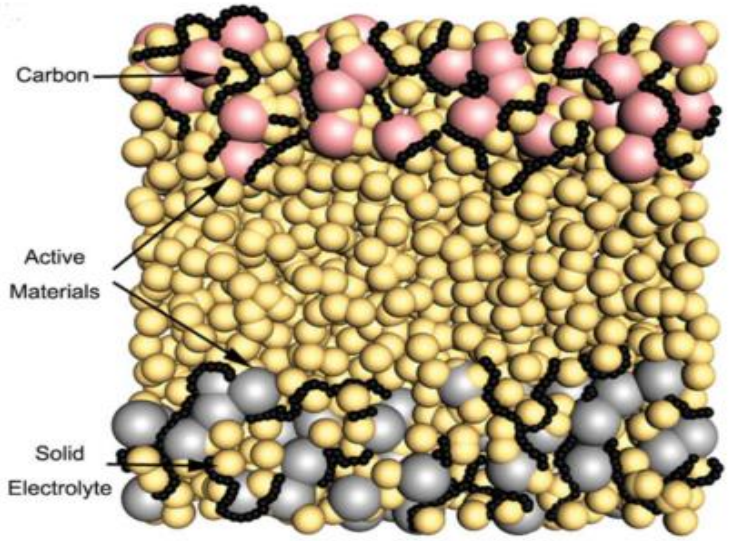

Figure 1.5. Schematic structure of a typical bulk-type all-solid-state lithium battery [19].

Moreover, only lithium ions are allowed to transfer in solid electrolyte so its transference number for lithium ions is almost 1. In addition, there is no concentration gradient problem which limits the cell current for solid electrolyte [20]. Considering these advantages, it is reasonable to replace the traditional organic electrolyte with solid electrolyte for next-generation batteries.

1.3.2 Solid State Electrolyte

Solid electrolyte can be categorized into two main types: one is polymer-based solid electrolyte and the other is inorganic solid electrolyte. Some common kind of polymer-based solid electrolytes include poly-ethylene oxide (PEO) [21], poly-acrylonitrile (PAN) [22], poly-methyl methacrylate (PMMA) [23] and so on. Armand *et al.* reported the ionic conductivity of PEO electrolyte could reach 10^{-5} S/cm at 40~60 ^{o}C in 1979 [24]. EVs based on the Li/PEO electrolyte/$LiFePO_4$ battery system has already been being under developed by Bollore Co., French and SEEO Co., US [25]. However, narrow temperature range, poor mechanical stability and low energy density are still intractable issues impeding the application of polymer-based solid state electrolyte [23]. In contrast, inorganic solid electrolytes have advantages of stable mechanical property, wide temperature window and non-flammability. It can be divided into two main groups: oxide solid electrolyte and sulfide solid electrolyte. Ionic conductivity is a key factor to evaluate if the material can be used as solid electrolyte for a battery system. The ionic conductivity of oxide solid electrolyte is usually low at room temperature due to the large resistance of solid oxide at ambient temperature [26]. $LaLiTiO_3$, a kind of oxide solid electrolyte, exhibits ionic conductivity in the range of 10^{-4}~10^{-3} S/cm at room temperature [27]. It is known that isovalent substitution of oxygen with sulfur and creation of an interfacial vacancy by aliovalent substitution are able to enhance the ionic conductivity of the solid electrolyte [28]. Kanno *et al.* reported that $Li_{10}GeP_2S_{12}$ which was a kind of crystalline sulfide solid electrolyte could reach a high ionic conductivity of $1.2*10^{-2}$ S/cm at room temperature [29]. As shown in Figure 1.6, the ionic conductivity of

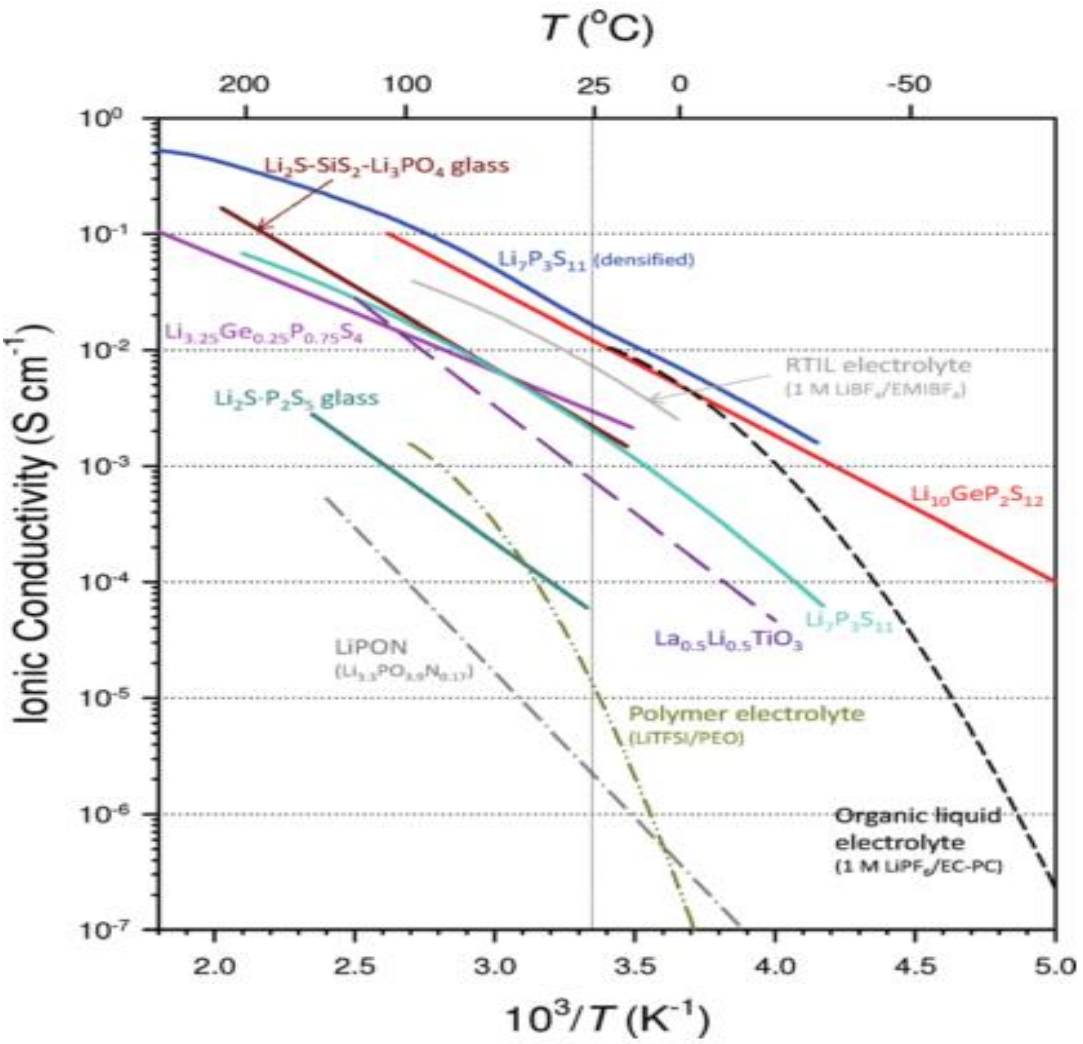

Figure 1.6. Ionic conductivity of several common solid electrolytes with respect to temperature compared with that of organic liquid electrolyte [20].

some inorganic solid electrolyte is comparable with that of traditional organic liquid electrolyte at elevated temperature (Fig.1.6). Under this circumstance, solid electrolyte actually owns higher lithium ion conductivity than liquid electrolyte because of its larger lithium ion transference number.

1.4 Inorganic Solid Electrolytes

1.4.1 Oxide Solid Electrolytes

I. Perovskite type structure

Perovskite structure is a structural family of inorganic material with a general structure of ABO_3 (Fig.1.7a). Alkaline earth metal ions (Ca^{2+}, Sr^{2+}, Ba^{2+}) are settled in A sites and transition metal ions (Ti^{4+}) are placed in B sites [30]. Brous *et al.* replaced the alkaline earth metal ions in A site with lithium ions and lanthanum ions and obtained perovskite structural $Li_{0.5}La_{0.5}TiO_3$ [31]. The transport of lithium ions in crystalline solid electrolyte is based on vacancy mechanism. The occupation of high-valence lanthanum ions leads to vacancies in A sites which improve the diffusivity of lithium ions. However, $Li_{0.5}La_{0.5}TiO_3$ is not commonly used as solid electrolyte due to its instability with lithium metal [32].

II. NASICON & LISICON type structures

NASICON stands for sodium super ionic conductor which has a general formula of $AM_2(BO_4)_3$ (Fig.1.7b). As illustrated in Figure 1.7b, A sites are occupied by alkali atoms (Li^+, Na^+, K^+, Rb^+), M sites are occupied by tetra-valence ions (Ti^{4+}, Zr^{4+}, Ge^{4+}, Sn^{4+}) and B sites are occupied by phosphorous ions [33]. LISICON, short for lithium super ionic conductor, can be gained by substituting sodium ions with lithium ions in A sites. Solid electrolytes with LISICON type structure have been investigated with intense interest because of their high chemical stability and wide electrochemical window at room temperature [34]. Morimoto *et al.* prepared $Li_{1.3}Ti_{1.7}Al_{0.3}(PO_4)_3$ by substituting Ti^{4+} with Al^{3+} for $LiTi_2(PO_4)_3$. Its ionic conductivity can reach the order of 10^{-4} S/cm at room temperature [35]. The

preparation process of NASICON and LISICON type solid electrolyte is complicated and needs to be optimized in the future [32].

III. Garnet type structure

The lithium containing garnet structure has a general formula of $Li_5La_3M_2O_{12}$ with M sites occupied by Nb or Ta (Fig.1.7c). Weppner *et al.* reported cubic-structure $Li_7La_3Zr_2O_{12}$ by replacing M sites with zirconium ions in 2007, showing a high ionic conductivity of $3*10^{-4}$ S/cm [36]. At room temperature, $Li_7La_3Zr_2O_{12}$ only exists with tetragonal structure which has lower conductivity of $1.63*10^{-6}$ S/cm [37]. The cubic structure can only be transferred from tetragonal structure at high temperature range between 100~150 ^{o}C. The research group led by Weppner also found a method to stabilize the cubic-structure at room temperature by Al doping [38]. Besides, garnet type solid electrolyte is stable with both air and lithium metal. It is a kind of suitable electrolyte candidate for ASSLBs [25].

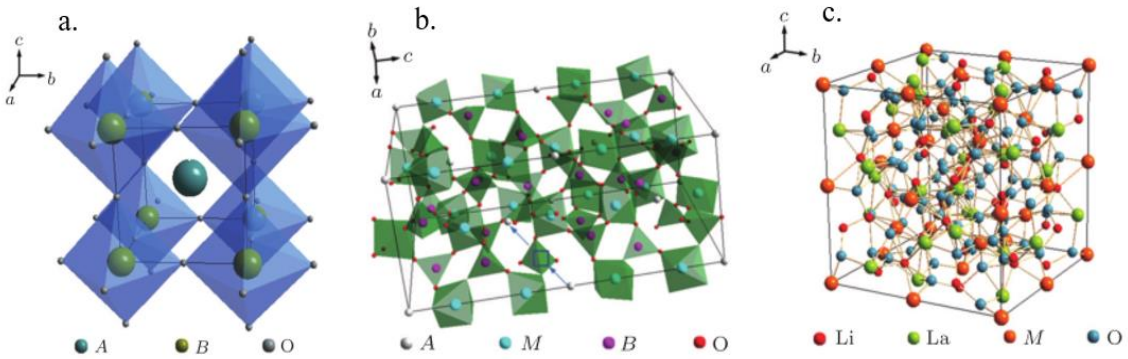

Figure 1.7. (a) Schematic structure of perovskite type solid electrolyte; (b) schematic structure of NASICON type solid electrolyte; (c) schematic structure of garnet type ($Li_5La_3M_2O_{12}$) solid electrolyte [32].

1.4.2 Sulfide Solid Electrolyte

Sulfide solid electrolytes have higher ionic conductivity (Fig.1.6) and better formability than oxide solid electrolytes. Hence, they can be prepared at room temperature by cold pressing without any heat treatment [39]. Sulfide solid electrolytes can be categorized into two different systems. One is Li_2S-SiS_2 based system and the other is Li_2S-P_2S_5 based system. Amorphous Li_2S-SiS_2 solid electrolyte can be prepared through high energy ball-milling, exhibiting ionic conductivity of $1.5*10^{-4}$ S/cm [40]. Kondo *et al.* doped Li_3PO_4 into the Li_2S-SiS_2 system and got samples with conductivity of $6.9*10^{-4}$ [41]. Li_2S-P_2S_5 system has been extensively studied owing to its high ionic conductivity. Li_2S-GeS_2-P_2S_5 with thio-LISICON type structure was found by Murayama *et al.* in 2001 [42]. Based on the

Table 1.1. Ionic conductivity of different kinds of sulfide solid electrolytes [39].

Composition	Conductivity at 25°C (S cm⁻¹)	Classification	Reference
$Li_{9.54}Si_{1.74}P_{1.44}S_{11.7}Cl_{0.3}$	2.5×10^{-2}	Crystal	(Kato et al. 2016b)
$Li_{10}GeP_2S_{12}$	1.2×10^{-2}	Crystal	Kamaya et al. (2011)
$Li_{10}SnP_2S_{12}$	4×10^{-3}	Crystal	Boron et al. (2013)
$Li_{3.833}Sn_{0.833}As_{0.166}S_4$	1.4×10^{-3}	Crystal	Sahu et al. (2014)
Li_6PS_5Cl	1.3×10^{-3}	Crystal	Boulineau et al. (2012)
$70Li_2S{\cdot}30P_2S_5$ ($Li_7P_3S_{11}$)	1.7×10^{-2}	Glass–ceramic	Seino et al. (2014)
$63Li_2S{\cdot}27P_2S_5{\cdot}10LiBr$	8.4×10^{-3}	Glass–ceramic	Ujiie et al. (2014)
$80Li_2S{\cdot}20P_2S_5$	1.3×10^{-3}	Glass–ceramic	Mizuno et al. (2006)
$30Li_2S{\cdot}26B_2S_3{\cdot}44LiI$	1.7×10^{-3}	Glass	Wada et al. (1983)
$50Li_2S{\cdot}17P_2S_5{\cdot}33LiBH_4$	1.6×10^{-3}	Glass	Yamauchi et al. (2013)
$63Li_2S{\cdot}36SiS_2{\cdot}1Li_3PO_4$	1.5×10^{-3}	Glass	Aotani et al. (1994)
$70Li_2S{\cdot}30P_2S_5$	1.6×10^{-4}	Glass	Zhang and Kennedy (1990)

LISICON type crystal structure, Kato *et al.* proposed that lithium super ionic conductor, $Li_{9.54}Si_{1.74}P_{1.44}S_{11.7}Cl_{0.3,}$ showed the highest ionic conductivity of $2.5*10^{-2}$ S/cm at room temperature as illustrated in Table 1.1 [43]. Using this kind of solid electrolyte material, high power density can be achieved by ASSLBs. Comparing with the crystal-structure oxide solid electrolyte, amorphous phase sulfide solid electrolyte have the advantage of low grain boundary resistance. The power density of ASSLBs is limited by ion transport not only in the bulk of solid electrolytes but also at the grain boundary. The grain boundary resistance is rate-determining in some oxide solid electrolytes with high ionic conductivity of 10^{-3} S/cm [44]. However, grain boundary resistance is considered to be negligible in amorphous sulfide solid electrolytes like Li_2S-P_2S_5 system. Li_3PS_4, $75Li_2S$-$25P_2S_5$ (mol %), has phase change with temperature increasing. Li_3PS_4 exists as γ-Li_3PS_4 phase under the temperature of 190 °C. When heating above 190 °C, it will change to β-Li_3PS_4 phase with a higher ionic conductivity [45]. In addition, the structure type also changes from amorphous glass to crystal glass-ceramic structure. The Li_2S-P_2S_5 system is not stable with air and water. It is prone to react with moisture and generate H_2S gas [46]. However, Hayashi *et al.* found that doping oxides in the Li_2S-P_2S_5 system could improve its chemical stability in nature [47]. The elimination of sintering process by using sulfide solid electrolyte brings the convenience for constructing bulk-type batteries.

1.5 Challenges of Further Development for ASSLBs

In order to further improve the performance of ASSLBs, two critical challenges need to be overcome: one is the large ionic resistance of the solid electrolyte and the other is the high interfacial resistance between the solid

electrolyte and electrodes [19]. The ionic resistance of solid electrolyte affects the mobility of lithium ion which is directly related to the power density of batteries. Crystalline solid electrolytes suffer the ionic resistance also from grain boundary. The interfacial resistance is mainly resulted from insufficient contact between the solid electrolyte and electrodes since the infiltrative property of solid electrolytes is not as good as that of liquid electrolyte. Consequently, the transport of lithium ions is restricted and the number of active sites for charge transfer reaction decreases [19]. Besides, most inorganic solid electrolytes are reduced at low potential and oxidized at intermediate potential easily. Therefore, the interphases need to be protected in order to stabilize the contact between the solid electrolytes and electrodes [48]. Lithium metal is supposed to be an ideal anode because of its high capacity and lowest potential (Fig.1.3). Unfortunately, the lithium dendritic growth during repeated cyclic dissolution and deposition of the lithium metal leads to internal short circuits in batteries using liquid electrolytes [49]. It is believed that the mechanical strength of solid electrolyte can suppress the formation of lithium dendrite. However, the lithium

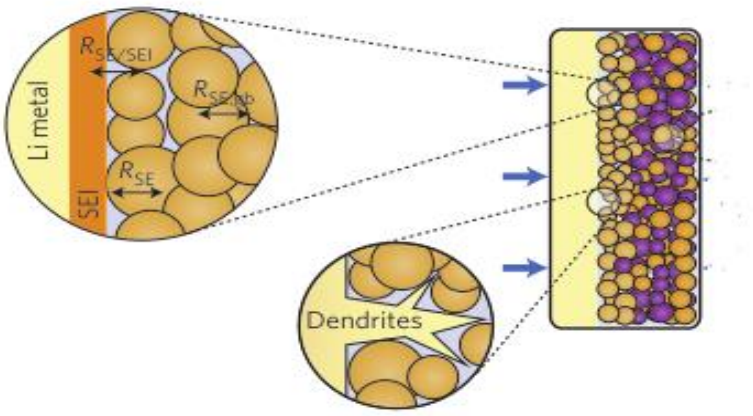

Figure 1.8. Schematic diagram of lithium dendrite growth in solid electrolytes [50].

dendrite is also observed in solid electrolytes. In crystalline solid electrolytes, lithium dendrites can grow along grain boundaries [50]. The SEI formed between the solid electrolyte and lithium anode also contribute some resistance to the whole ASSLB (Fig.1.8). This problem gets even worse for bulk-type ASSLBs with thicker electrodes and electrolytes.

LIB technology is already mature in current market but the safety concerns often arise since liquid electrolytes are combustible. ASSLB technology is considered to be an ideal alternative. However, the gravimetric energy density of ASSLBs is lower as solid electrolytes have higher density than liquid electrolytes. Therefore, the application of the ASSLB is favorable only if the use of either high-voltage cathode or high-capacity materials is allowed with solid electrolytes.

1.6 Objective of the Research Work

The objective of this research work is to develop an advanced solid electrolyte with comprehensively improved properties for bulk-type ASSLBs. Sulfide-based solid electrolyte was focused in this study because of its high ionic conductivity and excellent property. The goal of our study is to improve the performance of sulfide solid electrolyte from the following three aspects.

1). The improvement of the ionic conductivity of sulfide-based solid electrolyte at room temperature without heating treatment.

2). The improvement of interfacial stability between sulfide solid electrolyte and lithium metal anode.

3). The suppression of the lithium dendrite formation in sulfide solid electrolytes.

Lithium nitride (Li_3N) crystals have been attracted much attention due to their high ionic conductivity of $1.2*10^{-3}$ S/cm at room temperature. Unfortunately, it cannot be used as electrolyte directly since the decomposition voltage of Li_3N is around 0.445 V which is too low as an electrolyte [51]. Introducing nitrogen into Li_2S-SiS_2 based solid electrolyte has been reported to improve the ionic conductivity [52]. However, the effect of introducing nitrogen into Li_2S-P_2S_5 based sulfide solid electrolytes has not been systematically studied so far as we know. Herein, we try to dope nitrogen into Li_2S-P_2S_5 based sulfide solid electrolytes with Li_3N as the nitrogen source. The effects of doping nitrogen into sulfide solid electrolyte on ionic conductivity, interfacial stability with lithium metal, and dendrite formation are discussed in the following chapters.

Chapter 2: Theory and Experiment

2.1 Material Synthesis

A $75Li_2S$-$25P_2S_5$ (mol %) glass among Li_2S-P_2S_5 based sulfide solid electrolytes was used as a solid electrolyte in this research study. Different amounts of Li_3N were doped into the $75Li_2S$-$25P_2S_5$ solid electrolyte. The composition of the glass studied was written as $(75\text{-}1.5x)Li_2S$-$25P_2S_5$-xLi_3N (x=0, 3, 5, 8, 10, 20), where the Li/P ratio was kept constant (3:1). The doped nitrogen replaced some of the sulfur in $75Li_2S$-$25P_2S_5$ solid electrolyte. Li_2S (Sigma-Aldrich, 99%), P_2S_5 (Sigma-Aldrich, 99.98%) and Li_3N (Sigma-Aldrich, 99.5%) were used as the starting materials. These materials were weight in an argon (Ar)-filled glove box and loaded into a zirconia pot with 10 zirconia balls. The volume of the pot is 45 ml and the diameter of the zirconia balls is 10 mm. The pot was fixed in a planetary ball mill apparatus (PM 100; Retsch Gmbh). The rotation speed was set at 500 rounds per minute and the milling time was controlled for 15 hours to obtain glassy powder.

2.2 Powder Characterization

To identify the glassy powdered samples obtained by mechanical ball milling, X-ray diffraction (XRD) measurements were performed for the powdered samples. Powder X-ray pattern were obtained with a D8 Advance with LynxEye and SolX (Bruker AXS, WI, USA) using Cu K α radiation. The morphology of the prepared glassy powder was observed using a Hitachi a SU-70 field-emission scanning electron microscope. The results of powder characterization are illustrated in the next Chapter.

2.3 Electrochemical Measurement Technologies

2.3.1 Electrochemical impedance spectroscopy

Electrochemical impedance spectroscopy (EIS) is an useful technique for electrochemical characterization. The EIS is obtained by applying a small perturbation of the potential. The perturbation is a single sine wave or a superposition of a number of sine waves with different frequencies. The expression of results is composed of a real and an imaginary part. Then A "Nyquist plot" can be gained if the real part is plotted on Z-axis and the imaginary part is plotted on the Y axis (Fig.2.1). Low frequencies are on the left side and high frequencies are on the right [53]. The

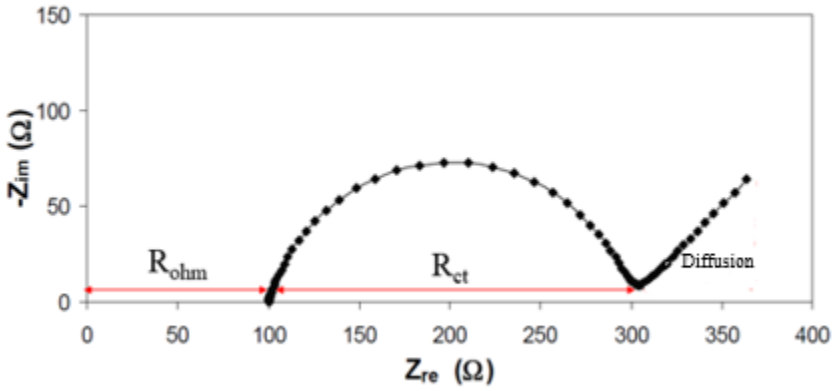

Figure 2.1. Schematic diagram of Nyquist plot consists of ohm resistance, charge transfer resistance and diffusion resistance.

plot consists of two parts: a depressed semicircle and an inclined line. The incline line at low frequency represents the diffusion of ions in electrodes. The depressed semicircle stands for the overlap of the SEI layer resistance and the interfacial charge transfer resistance. The length between the origin point and left-side point of the

depressed semicircle represents the ohmic resistance of the bulk electrolyte [54]. Based on the EIS technology, the resistance of different parts in the battery system can be distinguished.

2.3.2 Cyclic Voltammetry

The cyclic voltammetry (CV) is a common used technology of studying the electron transfer kinetics and transport properties of electrolysis reactions. For CV, a fixed range of potential is employed with a constant scan rate. The scan rate can be set manually and reflected on the slope of the potential with respect to time (Fig.2.2a). The characteristics of cyclic sweep voltammetry depends on the scan rate of voltage rate, the rate of the electron transfer reaction and the chemical reactivity of the electro-active species. The potential of the working electrode is measured against based on Figure 2.2 (b). In this region, the reduction process occurs. The resulting

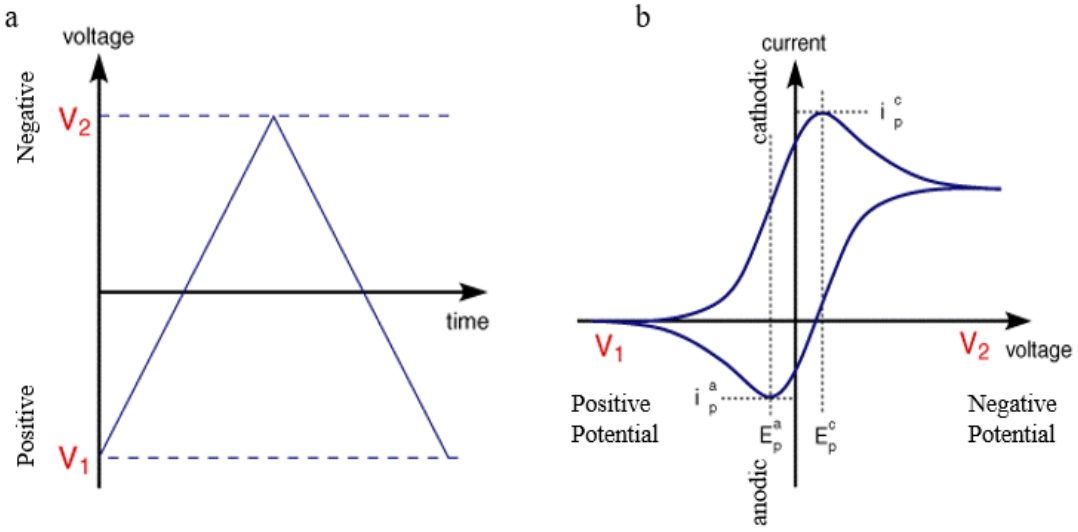

Figure 2.2. (a) The excitation signal of CV. (b) Schematic representative of CV with the potential versus reference electrode [55].

current is called cathodic current and the corresponding potential is called cathodic potential. The cathodic peak potential (E_p^c) is reached at some point. Then the CV scans from negative potential to positive potential. The oxidation process happens during this process, resulting anodic current and anodic potential. There is also an anodic peak potential (E_p^a) existing in this region [56]. The size of the area between the cathodic current curve and x-axis can be used to describe the extent of the reduction reaction. The reduction is more severe as the area gets larger.

2.4 Electrochemical Performance

The electrochemical performances of the milled powder were tested in a Swagelok cell which consists of two stainless steel rods and an insulating PTFE tank (Fig.2.3). The solid electrolyte and electrodes are cold-pressed at 360 MPa between the stainless steel rods inside the PTFE tank. In order to avoid any contact with air or moisture, the assembled Swagelok cell was coved by several layers of parafilm and tested outside the glove box.

The ionic conductivity of the solid electrolyte material can be calculated from the following equation:

$$\sigma = \frac{1}{\rho} = \frac{l}{R * A}$$

where σ represents the ionic conductivity of the solid electrolyte, ρ stands for the resistivity of the tested material, R is the electrical resistance of the material, l is the thickness of the pelletized sample and A is the cross-sectional area of the pelletized specimen. The thickness of the pelletized sample was measured by micrometer

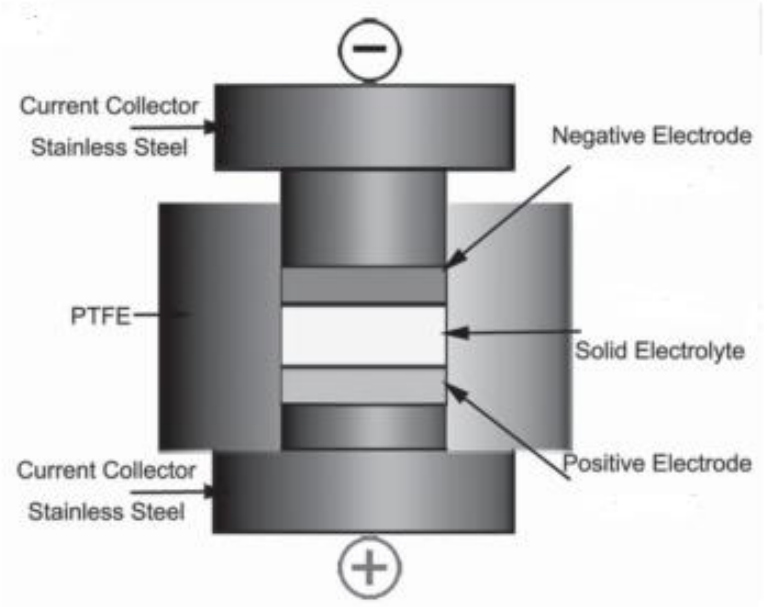

Figure 2.3. Schematic graph of the Swagelok cell configuration for all-solid-state battery test [19].

caliper. The cross-sectional area was gained based on the equation $S = \pi * (d/2)^2$ with the measured diameter of the cross section of the pelletized sample. The impedance of the sample material was measured using an electrochemistry workstation (Solartron 1287/1260) from 10^6 Hz to 0.01 Hz at room temperature.

The interfacial stability between the sulfide solid electrolyte and lithium metal anode was characterized by CV and EIS. The CV scanning was conducted on an electrochemical analyzer (CH Instruments, US). It was carried out for the pelletized sample using stainless steel rod as a working electrode and lithium metal as counter and reference electrode. The EIS measurement was carried out using symmetric cell configuration Li/solid electrolyte/Li in a Swagelok cell within the frequency range 10^6 Hz to 0.01 Hz. The cycle performance of the sulfide solid electrolyte was

evaluated at different current densities. The Swagelok cells were charged and discharged using a charge-discharge tester (CT2001A, Land, Wuhan).

Chapter 3: Results and Discussion

3.1 XRD and SEM Characterization

Li_2S, P_2S_5 and Li_3N are all crystal-structure inorganic compounds as the starting materials. The XRD patterns of (75-1.5x)Li_2S-25P_2S_5-xLi_3N (x = 0, 3, 5, 8, 10, 20 mol%) powders prepared by ball milling are depicted respectively (Fig. 3.1). There is no apparent crystalline peaks observed on the XRD patterns, indicating that amorphous glass is formed. It means that the mixture of the starting materials has reacted and achieved amorphous phase via ball milling in a planetary mill for 15 hours. The XRD result also provides the evidence that the nitrogen has been doped into the amorphous glass because no peaks for Li_3N can be observed. The surface

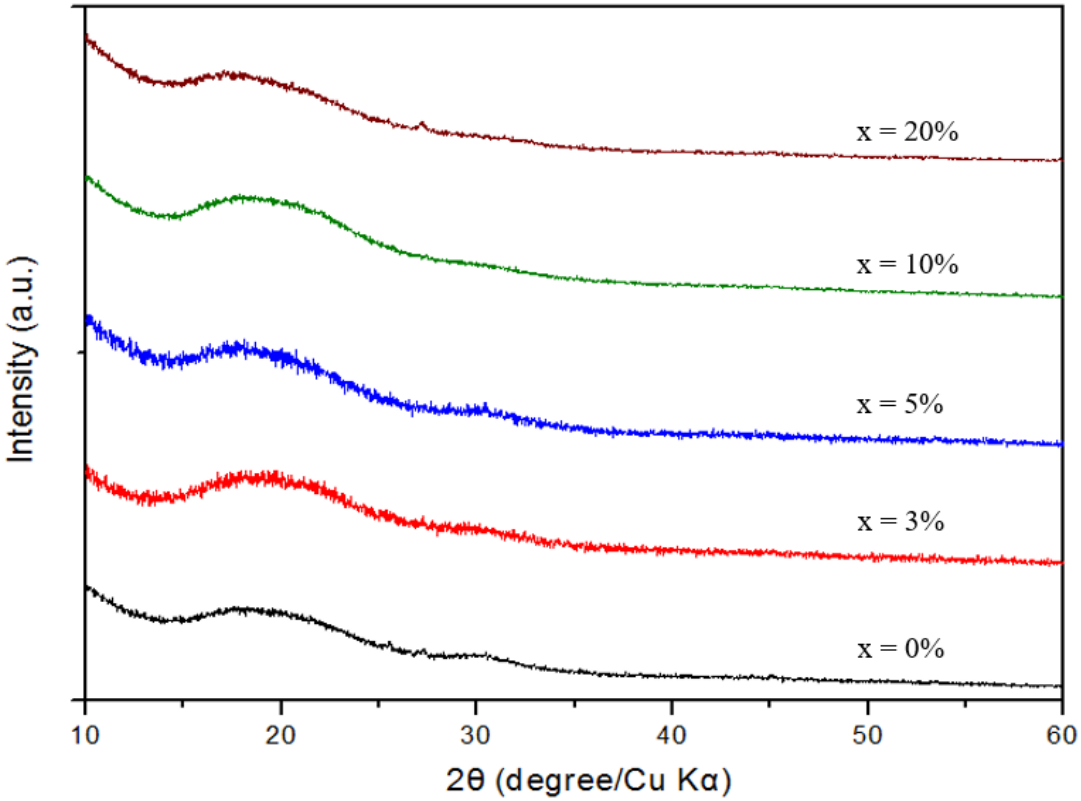

Figure 3.1. XRD patterns of (75-1.5x)Li_2S-25P_2S_5-xLi_3N amorphous powders after ball milling.

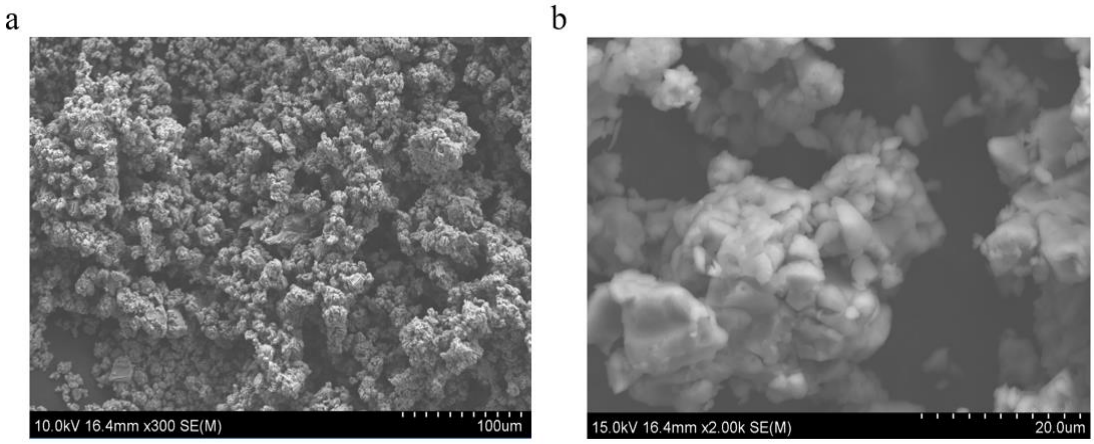

Figure 3.2. Secondary electron SEM image of (a) LPSN powder under low magnification and (b) LPSN powder under high magnification.

morphology of the ball-milled powders were characterized by the SEM shown in Fig.3.2a. It is observed that the particle size of solid electrolyte is only about twenty microns after ball milling at room temperature (Fig.3.2 b).

3.2 Measurements of Ionic Conductivity

The ionic conductivity of the synthesized solid electrolyte material was measured in the symmetric electron-blocking cell configuration at room temperature. The symmetric electron-blocking cell configuration consists of the solid electrolyte in the middle and inert electrodes on both sides. We chose the stainless steel as the inert electrode since it has no reaction with sulfide solid electrolyte. The cell configuration was designed as stainless steel/solid electrolyte/stainless steel for the conductivity measurement. The ball-milled powder was pelletized in a Swagelok cell whose stainless steel rods can be used as electrodes. The stainless steel rods of the Swagelok cell was polished before cell assembling in order to improve their contact with the

solid electrolyte. Several layers of parafilm was twined around the assembled Swagelok cell before taking the cell out of the glove box for impedance measurement. The impendence of nitrogen-doped $75Li_2S$-$25P_2S_5$ solid electrolyte was measured in the frequency range 10^6 Hz to 0.01 Hz at room temperature (Fig.3.3). The high

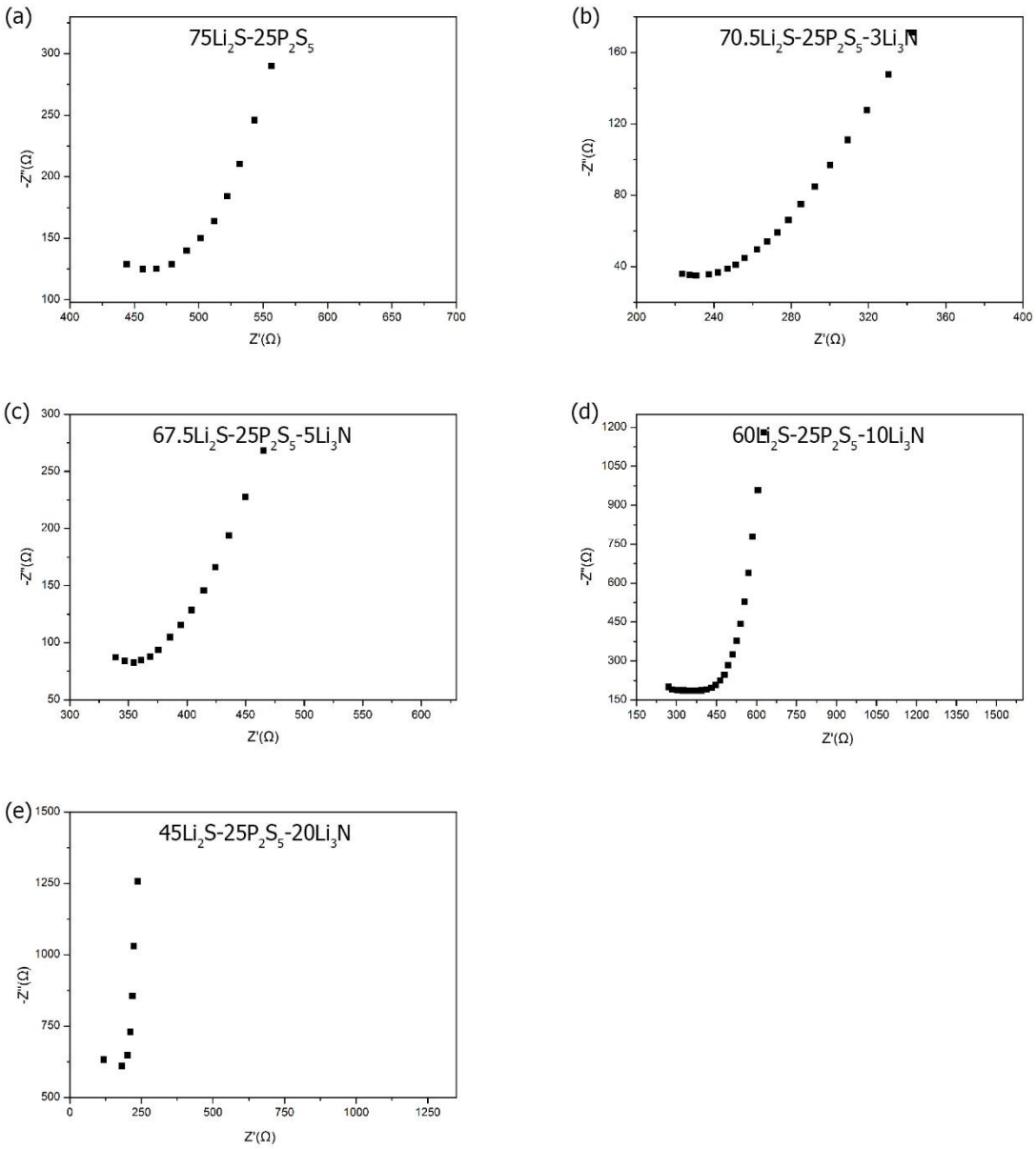

Figure 3.3. Impedance spectra of nitrogen-doped sulfide solid electrolyte tested in (stainless steel)/solid electrolyte / (stainless steel) configuration at room temperature.

frequency region from the origin point to the lowest point of the impedance curve represents the impedance of bulk of the electrolyte. After finishing the impedance measurement, the Swagelok cell was disassembled for measuring the thickness and cross-sectional diameter of the pelletized sample. With the measured data of pellet's thickness and calculated value of pellet's cross-sectional area, the ionic conductivity can be obtained via the equation in section 2.4. The values of the ionic conductivity of $75Li_2S$-$25P_2S_5$ based solid electrolyte with different amount of nitrogen doping are shown in Table 3.1. The results shows that the ionic conductivity of all the sulfide solid electrolyte gets enhanced after nitrogen doping at room temperature. Among

Table 3.1. The room-temperature ionic conductivity of sulfide solid electrolytes doped by different amount of nitrogen.

Sulfide solid electrolyte	$75Li_2S$-$25P_2S_5$	$70.5Li_2S$-$25P_2S_5$-$3Li_3N$	$67.5Li_2S$-$25P_2S_5$-$5Li_3N$
Thickness of pellet (cm)	0.085	0.086	0.087
Cross-sectional area (cm^2)	0.866	0.866	0.866
Ionic conductivity (S/cm)	$2.15*10^{-4}$	$4.30*10^{-4}$	$2.84*10^{-4}$
Sulfide solid electrolyte	$60Li_2S$-$25P_2S_5$-$10Li_3N$	$45Li_2S$-$25P_2S_5$-$20Li_3N$	
Thickness of pellet (cm)	0.093	0.098	
Cross-sectional area (cm^2)	0.866	0.866	
Ionic conductivity (S/cm)	$2.90*10^{-4}$	$6.22*10^{-4}$	

them, 20% nitrogen-doped sulfide solid electrolyte shows the largest ionic conductivity which is almost three times as the one without nitrogen doping. The enhancement of ionic conductivity is due to the high ionic conductivity of Li_3N with $1.2*10^{-3}$ S/cm at room temperature. The result does not show a trend that the ionic conductivity increases with the increasing amount of doped nitrogen. For instance, the ionic conductivity of 5% nitrogen-doped $75Li_2S$-$25P_2S_5$ solid electrolyte is not larger than that of 3% nitrogen-doped sample. This may needs further investigation for seeking the reason.

3.3 Interfacial Stability between Lithium Metal Anode and Solid Electrolyte

The interfacial stability was characterized by EIS and CV technologies. The EIS measurements were also performed in electronically blocking cell arrangements. For the sake of studying the interfacial stability of nitrogen-doped solid electrolyte with lithium metal, a Li/solid electrolyte/Li cell configuration was used with lithium metal on both sides of the pelletized solid electrolyte. There is only the Li/solid electrolyte interface presenting in such symmetrical cell configuration. Figure 3.4 shows the impedance measurement carried out in the frequency range of 10^6 Hz to 0.01 Hz at room temperature. All the sulfide solid electrolytes with different amount of nitrogen doping were pelletized and tested in the same Swagelok in order to eliminate any external influence. As mentioned in section 2.3.1, the semicircle of the impedance plot represents the interfacial resistance between the solid electrolyte and lithium metal anode. The interfacial resistance gets largely reduced as the diameter of the semicircle becomes much smaller after nitrogen doping. The interfacial resistance is about 480 Ω for $75Li_2S$-$25P_2S_5$ solid electrolyte without any nitrogen doping. It

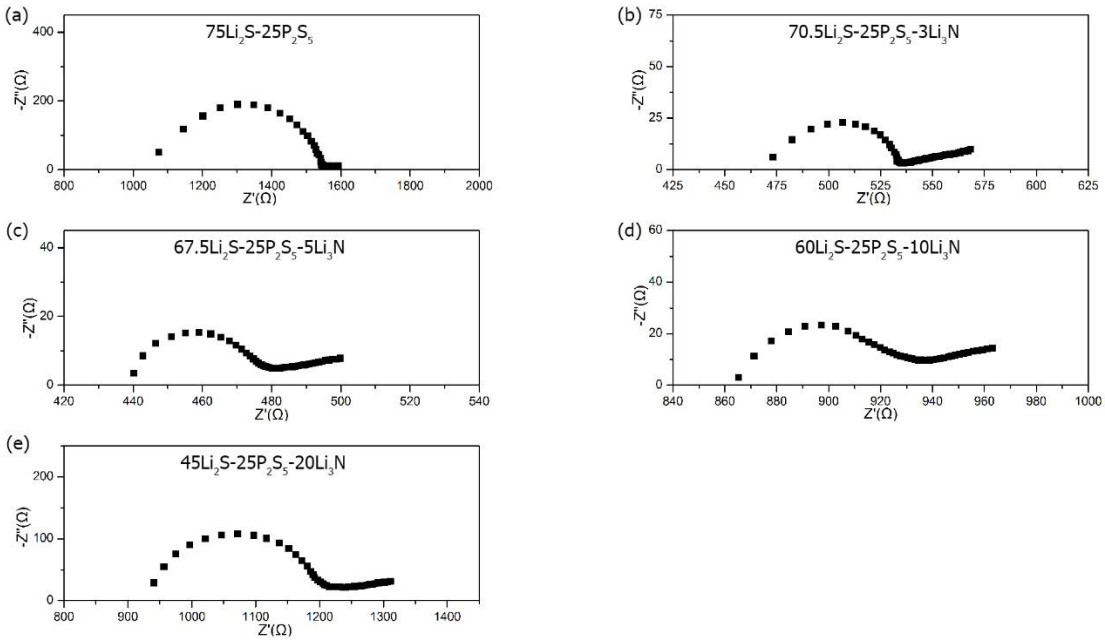

Figure 3.4. The impendence plots of the Li/solid electrolyte/Li symmetric cell configuration at room temperature.

decreases to 60, 40, 75 and 275 Ω corresponding to 3%, 5%, 10% and 20% nitrogen doping. The apparent reduction of the interfacial resistance indicates the interfacial stability between the lithium metal anode and sulfide solid electrolyte gets largely improved after nitrogen doping. The 5% nitrogen-doped sulfide solid electrolyte shows the largest interfacial resistance reduction from 480 to 40 Ω. The reason why the interfacial stability gets improved is because a more stable chemical compound is generated at the Li/sulfide solid electrolyte interface. The $75Li_2S$-$25P_2S_5$ solid electrolyte is not stable with the lithium metal due to its narrow potential window. It decomposes and generates Li_2S and Li_3P, forming a layer of solid electrolyte interface (SEI) [57]. However, this SEI layer is not ionic conductive, which leads to a large resistance. The decomposing product of nitrogen-doped sulfide solid electrolyte

is Li_2S, Li_3P and Li_3N. Li_3N is a compound which is thermodynamically stable with the lithium metal, and is an ionic conductor [58]. Introducing Li_3N in the SEI layer can strongly improve the interfacial stability between the lithium metal anode and solid electrolyte. As a consequence, the interfacial resistance gets reduced after nitrogen doping reflected from the impedance plots.

Due to the existence of decomposition reaction of solid electrolyte, we leave all the assembled Swagelok cell in the glove box for 10 hours before doing the EIS test in order to let the reaction finish completely. However, the physical press for pelletizing the solid electrolyte with lithium metal anode cannot provide an intimate contact. Herein, we processed five charge-discharge cycles with 14 $\mu A/cm^2$ constant current density to improve the contact. During the charge and discharge process, the lithium dissolution and deposition reactions occur. The contact area between the lithium metal anode and solid electrolyte gets enlarged. The decomposition process of solid electrolyte takes place as soon as it contacts with lithium metal. Consequently, more Li_3N is produced in the SEI layer and the SEI layer gets further stabilized. As shown in Figure 3.5, the interfacial resistance gets further reduced after five constant-current charge-discharge cycles. It decreases from 60 to 30 Ω, 40 to 20 Ω, 75 to 50 Ω and 275 to 90 Ω for 3%, 5%, 10% and 20% nitrogen-doped $75Li_2S$-$25P_2S_5$ solid electrolyte, respectively (Fig.3.5).

The improvement of the interfacial stability could be supported by cyclic voltammetry (CV) results as well. The CV test was conducted using a Li/solid electrolyte/stainless steel cell configuration, where the stainless steel rods worked as working electrode and the lithium metal worked as counter and reference electrodes.

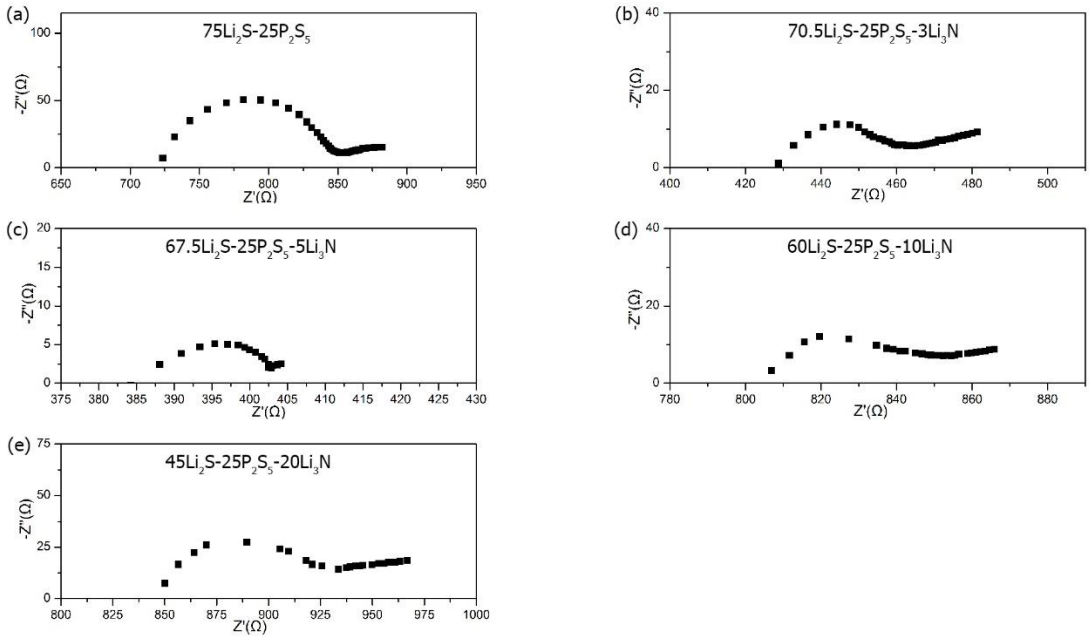

Figure 3.5. The impendence plots of the Li/solid electrolyte/Li cell after five constant-current charge-discharge cycles at room temperature.

All the CV tests were conducted in the same Swagelok cell since the CV results could be affected by the properties of the tested cell such as the roughness of the stainless steel rods. The potential difference between stainless steel and lithium metal is around 2V. Thus, the CV measurement was scanned from 2V to 0V and then back to 2V with a scan rate of 0.1 mV/s. The cathodic peak of the CV curve stands for the reduction decomposition of the sulfide solid electrolyte at low voltage. Figure 3.6a and Figure 3.6b shows the peaks gets smaller for all the nitrogen-doped $75Li_2S$-$25P_2S_5$ solid electrolyte, implying the sulfide solid electrolyte becomes more electrochemical stable with lithium metal after nitrogen doping. In addition, the $75Li_2S$-$25P_2S_5$ solid electrolyte with 5% nitrogen doping shows the best performance with the smallest peak among all the tested samples. The result shows the feasibility of applying the

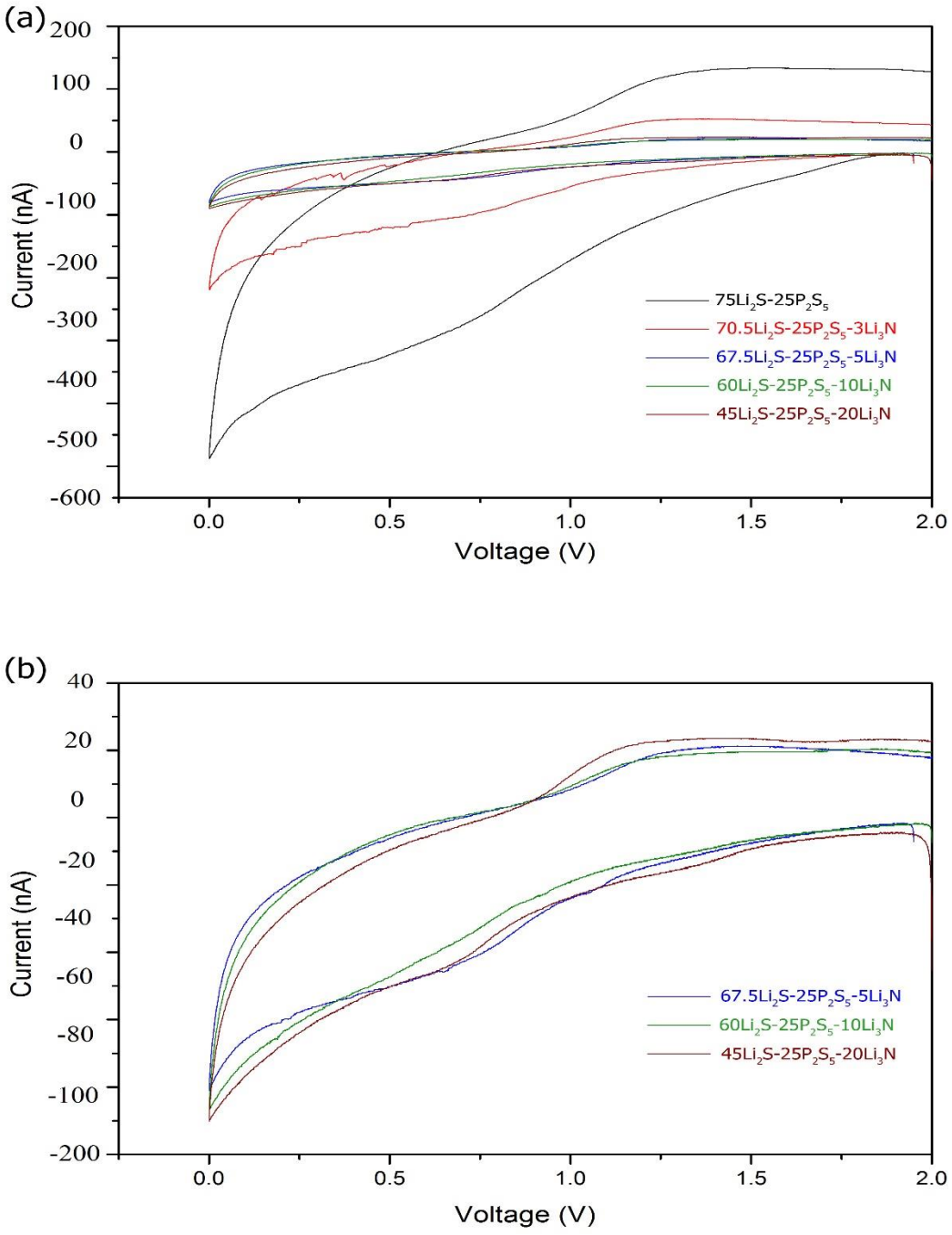

Figure 3.6. (a) The CV measurement of Li/solid electrolyte/stainless steel cell in the voltage range between 2V and 0V with the scan rate of 0.1 mV/s. (b) Magnification of the CV curve for 5%, 10% and 20% nitrogen-doped sulfide solid electrolyte.

nitrogen doping method in amorphous sulfide solid electrolyte for improving its interfacial stability with lithium metal anode.

3.4 Lithium Dendrite Suppression in the N-doped Sulfide Electrolyte

The suppression ability of the solid electrolyte to lithium dendritic growth was tested in a Li/solid electrolyte/Li cell configuration at room temperature. The lithium dendrite is formed during the dissolution and deposition process of lithium metal, causing internal short circuits. Before conducting the measurement of control ability of the lithium dendritic growth, the assembled Swagelok cell was left in glove box for 10 hours and run five galvanostatic charge-discharge cycles. The cell was tested under a gradually increasing current density. The tested current density started at 56 $\mu A/cm^2$ and increased by 42 $\mu A/cm^2$ for the next charge-discharge cycle. Figure 3.8 shows the relationship between the voltage and increasing current density for each solid electrolyte with different amount of nitrogen doping. The $75Li_2S$-$25P_2S_5$ solid electrolyte is able to hold a maximum current density of 183 $\mu A/cm^2$ at room temperature. The voltage drops when the current density reaches above this value. In order to study the detailed reason for the voltage drop, EIS was used to help analyze the phenomenon. The EIS measurement data for $75Li_2S$-$25P_2S_5$ solid electrolyte was recorded before running the charge-discharge cyclic test with gradually increasing current density. It was recorded again as soon as the voltage dropped. The impedance results under these two different conditions were shown in Figure 3.8a and Figure 3.8b. As illustrated in the figure, the bulk resistance of the solid electrolyte gets reduced from 725 to 320Ω and the semicircle disappears in the second figure. The large reduction of the electrolyte bulk and the disappearance of the

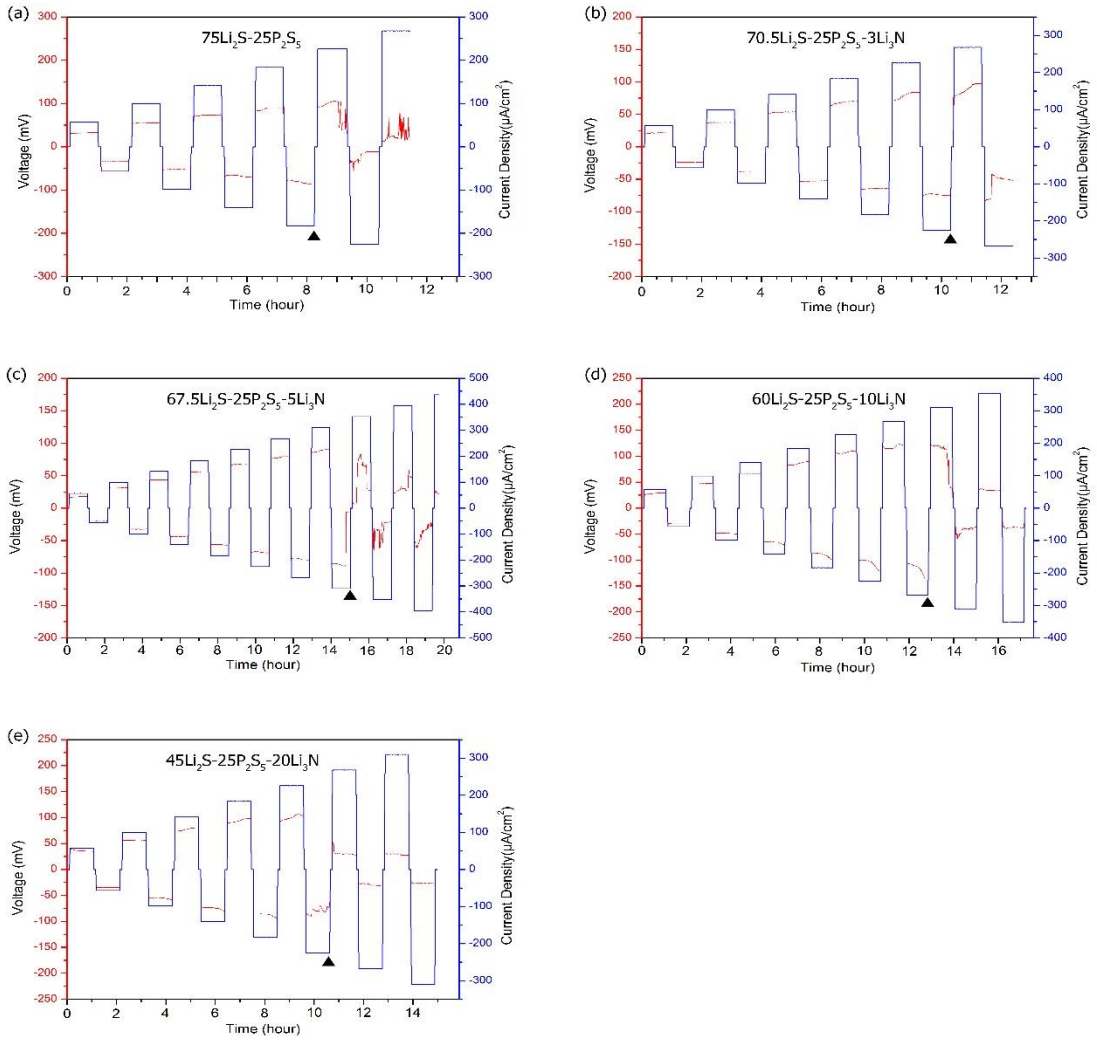

Figure 3.7. Charge-discharge cyclic test with increasing current density for Li/solid electrolyte/Li cells at room temperature.

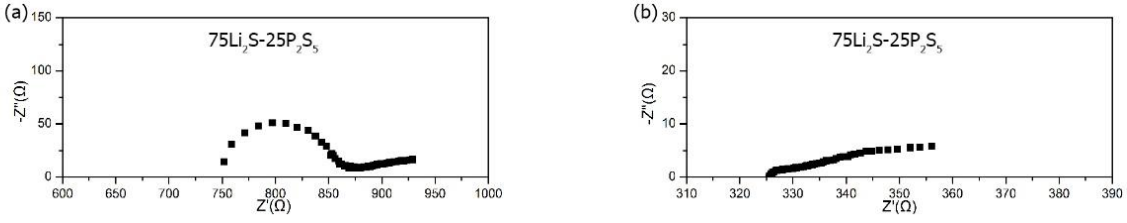

Figure 3.8. Impedance plots of Li/solid electrolyte/Li cells (a) before the increasing current-density test (b) after the voltage drops.

semicircles of charge transfer resistance is caused by the onset of lithium dendritic growth. When the lithium dendrite starts to form, it is analogical to move the lithium metal electrodes towards each other. Thus, the distance between the two lithium metal electrodes becomes smaller and the resistance of electrolyte bulk becomes smaller. However, the interface between the dendritic lithium and solid electrolyte is rough since the lithium dendrite is formed randomly. As a result, the interfacial stability becomes lower and interfacial resistance becomes larger. The disappearance of semicircle is because its radius becomes too large so the semicircle is not able to be presented in our frequency range.

In terms of the experimental data, the critical current density for lithium dendrite onset is showed as 225, 310, 268 and 225 $\mu A/cm^2$ corresponding to 3%, 5%, 10% and 20% nitrogen-doped sulfide solid electrolyte (Fig.3.7). Comparing with the $75Li_2S$-$25P_2S_5$ solid electrolyte, the critical current density for lithium dendrite onset of sulfide solid electrolyte gets enhanced in a range of 23% to 70% with different amount of nitrogen doping. It means the existence of nitrogen slows down the speed of lithium dendritic growth since the nitrogen in the solid electrolyte can react with lithium metal. Thus, some of the lithium dendrite reacts with the nitrogen and its growth got suppressed. The analysis is further confirmed by the direct constant current test using the same cell configuration (Fig.3.9). The constant current density was set as 140 $\mu A/cm^2$ for twenty cycles. The EIS analysis was followed after the constant current test. The $75Li_2S$-$25P_2S_5$ solid electrolyte can only sustain for five cycles and then the voltage has a sudden drop to a very low value. The impedance plot shows the cell is internal short after the cycling test (Fig.3.10a). Such situation

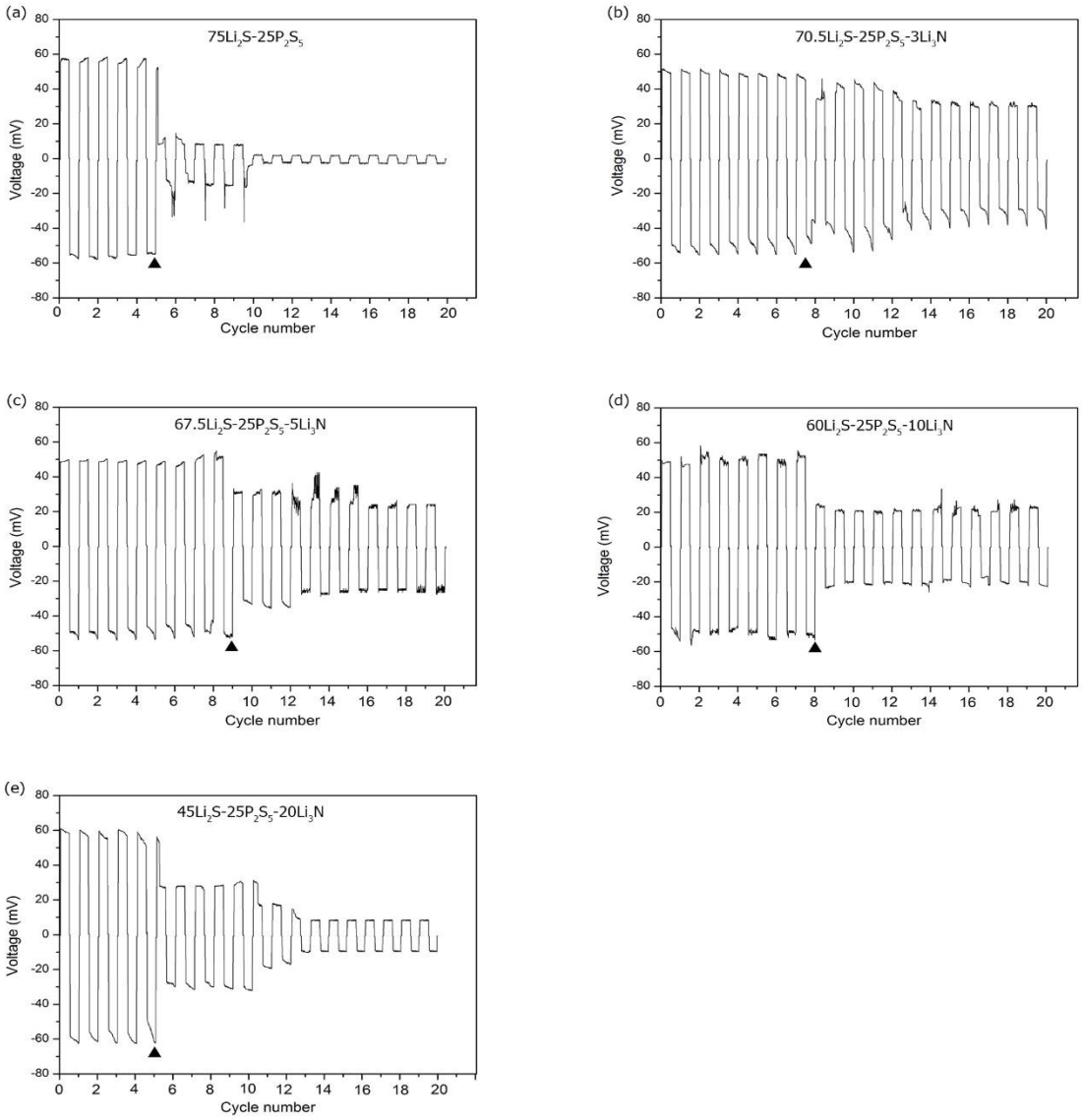

Figure 3.9. The cycling performance to the Li/solid electrolyte/Li cells.

does not happen to the nitrogen-doped sulfide solid electrolyte. Their impedance measurements shows the lithium dendrite starts to grow as the voltage drops. However, the lithium dendrite is not able to penetrate the solid electrolyte to cause battery short circuit. It provides the evidence that the existence of nitrogen in sulfide solid electrolyte can effectively suppress the growth of lithium dendrite. The sulfide

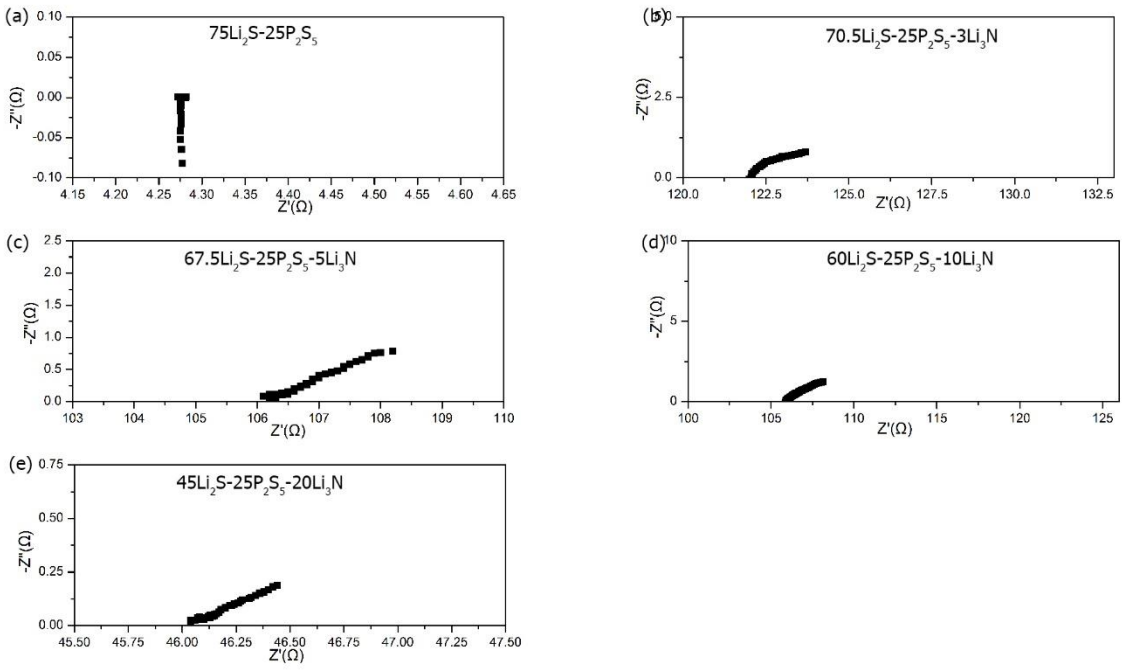

Figure 3.10. Impedance plots of Li/solid electrolyte/Li cell after 20 galvanostatic charge-discharge cycles at room temperature.

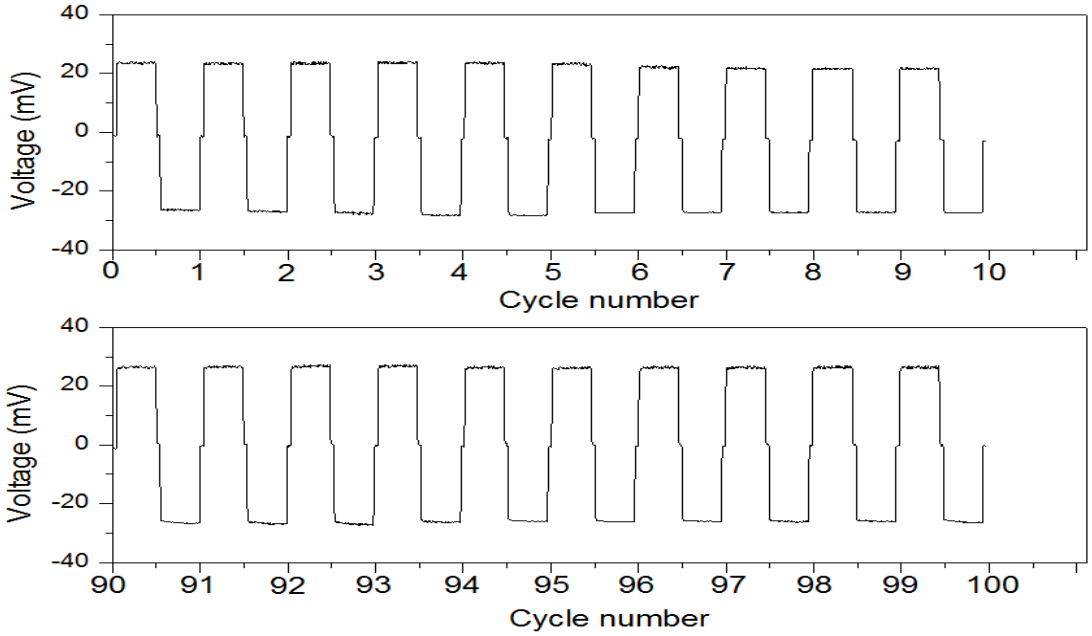

Figure 3.11. The durable cycling performance of constant current charge-discharge test in Li/(67.5Li_2S-25P_2S_5-5Li_3N)/Li cells at room temperature.

solid electrolyte with 5% nitrogen-doping shows a current density for lithium dendrite onset is 310 $\mu A/cm^2$ and durable cycling number for the constant current density test approaches 10 cycles. The results show that the best suppression performance to the onset of lithium dendrite is achieved by the sulfide solid electrolyte with 5% nitrogen doping. It indicates that only appropriate amount of nitrogen doping is able to maximize the benefit to the sulfide solid electrolyte.

In order to check the long-term stability of the 5% nitrogen-doped solid electrolyte with the lithium metal anode, a galvanostatic charge-discharge cycling test with constant current density of 70 $\mu A/cm^2$ was conducted at room temperature (Fig.3.11). The experimental result shows that the voltage does not drop even after 100 cycles. The voltage of the first ten cycles and the last ten circles of the cycling test is very consistency, implying very good electrochemical stability between the 5% nitrogen-doped sulfide solid electrolyte and lithium metal under this current density.

Chapter 4: Conclusion

The study of doping nitrogen in sulfide solid electrolyte shows comprehensive improvements in ionic conductivity, interfacial stability with lithium metal anode and suppression ability to lithium dendrite growth. The ionic conductivity is enhanced as large as two times for 20% nitrogen-doped $75Li_2S$-$25P_2S_5$ solid electrolyte. The enhancement of ionic conductivity comes from the high ionic conductivity of Li_3N at room temperature. The $75Li_2S$-$25P_2S_5$ solid electrolyte with 5% nitrogen doping shows a reduction over 80% in the interfacial resistance between Li anode and solid electrolyte. The improvement of interfacial stability is due to the thermodynamic stability between the Li_3N and lithium metal. The dendrite formation in solid electrolyte could be effectively suppressed by 5% nitrogen-doped $75Li_2S$-$25P_2S_5$ solid electrolyte with the critical current density enhanced by 70%. Its good suppression ability to the lithium dendritic growth is owing to the reaction between lithium and nitrogen. Besides, the experiment results show that the amount of nitrogen doped into the solid electrolyte should be chosen appropriately in order to maximize its benefit. According to the abovementioned enhancements, nitrogen doping is an efficient and effective way to improve the performance of sulfide solid electrolyte.

Chapter 5: Future Work

1. Further investigation is needed in studying the reason why the trend of improving ionic conductivity of nitrogen-doped sulfide solid electrolyte is not linear.

2. Based on the experiment results, the 5% nitrogen-doped sulfide solid electrolyte showed the best performance in interfacial stability with lithium metal anode and the suppression of the growth of lithium dendrite. The specific reason for why the sulfide solid electrolyte with 5% nitrogen doping having better performance than 10% or 20% nitrogen-doped sulfide solid electrolyte is needed to be investigated in future study.

3. The solid electrolyte has better performance at elevated temperature. The test performance of nitrogen-doped sulfide solid electrolyte at high temperature has not been demonstrated in this thesis. In the future study, we need to test our nitrogen-doped sulfide solid electrolyte with the cell configuration of Li/solid electrolyte/Li at the temperature range between 60 and 100 ℃.

Bibliography

[1]. Poizot, P. & Dolhem, F. Clean energy new deal for a sustainable world: from non-CO2 generating energy sources to greener electrochemical storage devices. Energy Environ. Sci. 4, 2003 (2011).

[2]. Tarascon, J.-M. & Armand, M. Issues and challenges facing rechargeable lithium batteries. Nature 414, 359–367 (2001).

[3]. Armand, M. & Tarascon, J.-M. Building better batteries. Nature 451, 652–657 (2008).

[4]. Manthiram, A. Materials Challenges and Opportunities of Lithium Ion Batteries. J. Phys. Chem. Lett. 2, 176–184 (2011).

[5]. K. Mizushima; P.C. Jones; P.J. Wiseman; J.B. Goodenough. $LiCoO_2$ ($0<x<1$): A New Cathode Material for Batteries of High Energy Density. *Materials Research Bulletin*. 15: 783–789 (1980).

[6]. Hunter, J. C. Preparation of a new crystal form of manganese dioxide: λ-MnO2. J. Solid State Chem. 39, 142–147 (1981).

[7]. Chung, S.-Y., Bloking, J. T. & Chiang, Y.-M. Electronically conductive phospho-olivines as lithium storage electrodes. Nat. Mater. 1, 123–128 (2002).

[8]. Park, C.-M., Kim, J.-H., Kim, H. & Sohn, H.-J. Li-alloy based anode materials for Li secondary batteries. Chem. Soc. Rev. 39, 3115–3141 (2010).

[9]. Idota, Y. Tin-Based Amorphous Oxide: A High-Capacity Lithium-Ion-Storage Material. Science (80-.). 276, 1395–1397 (1997).

[10]. Ng, S. H. et al. Highly reversible lithium storage in spheroidal carbon-coated silicon nanocomposites as anodes for lithium-ion batteries. Angew. Chemie - Int. Ed. 45, 6896–6899 (2006).

[11]. Besenhard, J. O., Heydecke, J., Wudy, E., Fritz, H. P. & Foag, W. Characteristics of molybdenum oxide and chromium oxide cathodes in primary and secondary organic electrolyte lithium batteries. Part II. Transport properties. Solid State Ionics 8, 61–71 (1983)

[12]. Goodenough, J. B. & Kim, Y. Challenges for rechargeable batteries. J. Power Sources 196, 6688–6694 (2011).

[13]. Xu, K. Nonaqueous liquid electrolytes for lithium-based rechargeable batteries. Chem. Rev. 104, 4303–4417 (2004).

[14]. Rosamar á Fong, Ulrich von Sacken, J. R. Dahn. Studies of lithium intercalation into carbons using nonaqueous electrical cells. J. Electrochem. Soc. 137, 2009–2013 (1990).

[15]. Wu Li, J. R. Dahn, D. S. Wainwright. Rechargeable Lithium Batteries with Aqueous Electrolytes. Science. Vol. 264, Issue 5162, pp. 1115-1118 (1994)

[16]. Seino, Y., Ota, T., Takada, K., Hayashi, A. & Tatsumisago, M. 16,A sulphide lithium super ion conductor is superior to liquid ion conductors for use in rechargeable batteries. Energy Environ. Sci. 7, 627–631 (2014).

[17]. Nagao, M., Kitaura, H., Hayashi, A. & Tatsumisago, M. Characterization of all-solid-state lithium secondary batteries using CuxMo6S8-y electrode and Li2S-P2S5 solid electrolyte. J. Power Sources 189, 672–675 (2009).

[19]. Han, F., Gao, T., Zhu, Y., Gaskell, K. J. & Wang, C. A battery made from a single material. Adv. Mater. 27, 3473–3483 (2015).

[20]. Jung, Y. S., Oh, D. Y., Nam, Y. J. & Park, K. H. Issues and challenges for bulk-type all-solid-state rechargeable lithium batteries using sulfide solid electrolytes. Isr. J. Chem. 55, 472–485 (2015).

[21]. Wright P. V． Electrical conductivity in ionic complexes of poly(ethylene oxide)． British Polymer Journal，7(5)： 319—327．(1975)

[22]. Appetecchi, G. B. & Scrosati, B. ELECTROCHEMICAL SOCIETY LETTERS Ambient-Temperature, Rechargeable, All-Solid Lithium/Polypyrrole Polymer Battery. 142, 2–3 (1995).

[23]. S. S. Zhang, M. H. Ervin, K. Xu, T. R. Jow. Microporous poly(acrylonitrile-methyl methacrylate) membrane as a separator of rechargeable lithium battery Electrochim. Acta 49, 3339 (2004)

[24]. Armand M. B., Chabagno J. M., Duclot M J. Fast ion transport in solids-electrodes and electrolytes. Amsterdam: Elsevier; (1979)

[25]. Zhang, S., Wang, S., Ling S., Gao, J., Wu, J., Xiao, R., Li, H. & Chen, L. Fundamental scientific aspects of lithium ion batteries: All-solid-state lithium-ion batteries. Energy Storage Science and Technology. Vol. 3: No.4 (2014)

[26]. Kim, J. G. et al. A review of lithium and non-lithium based solid state batteries. J. Power Sources 282, 299–322 (2015).

[27]. Inaguma, Y., Katsumata, T., Itoh, M. & Morii, Y. Crystal Structure of a Lithium Ion-Conducting Perovskite La2/3−xLi3xTiO3 (x=0.05). J. Solid State Chem. 166, 67–72 (2002).

[28]. Kanno, R. & Murayama, M. Lithium Ionic Conductor Thio-LISICON: The Li2S-GeS2-P2S5 System. J. Electrochem. Soc. 148, A742 (2001).

[29]. Kamaya, N. et al. A lithium superionic conductor. Nat. Mater. 10, 682–6 (2011).

[30]. Bhalla, A. S., Guo, R., & Roy, R. The perovskite structure - A review of its role in ceramic science and technology. Materials Research Innovations, 4(1), 3-26 (2000).

[31]. Brous J, Fankuchen I, Banks E. Rare earth titanates with a perovskite structure. Acta Crest. 6(1): 67-70 (1953).

[32]. Yao, X. et al. All-solid-state lithium batteries with inorganic solid electrolytes: Review of fundamental science. Chin. Phys. B 25, 18802 (2016).

[33]. Lars-Oven Hagman, Peder Kierkegaard. The crystal structure of $NaMe^{IV}_2(P0_4)_3$; Me^{IV}=Ge, Ti, Zr. Aeta Chemica Scandinavica, 22(6): 1822. 1832 (1968).

[34]. Thangadurai, V. & Weppner, W. Recent progress in solid oxide and lithium ion conducting electrolytes research. Ionics (Kiel). 12, 81–92 (2006).

[35]. Morimoto, H. et al. Preparation of lithium ion conducting solid electrolyte of NASICON-type Li1+xAlxTi2-x(PO4)3 (x = 0.3) obtained by using the mechanochemical method and its application as surface modification materials of LiCoO2 cathode for lithium cell. J. Power Sources 240, 636–643 (2013).

[36]. Murugan, R., Thangadurai, V. & Weppner, W. Fast lithium ion conduction in garnet-type Li7La 3Zr2O12. Angew. Chemie - Int. Ed. 46, 7778–7781 (2007).

[37]. Awaka, J., Kijima, N., Hayakawa, H. & Akimoto, J. Synthesis and structure analysis of tetragonal Li7La3Zr2O12 with the garnet-related type structure. J. Solid State Chem. 182, 2046–2052 (2009).

[38]. Geiger, C. A. et al. Crystal chemistry and stability of ‘Li7La3Zr2O12’ garnet: A fast lithium-ion conductor. Inorg. Chem. 50, 1089–1097 (2011).

[39]. Hayashi, A., Sakuda, A. & Tatsumisago, M. Development of Sulfide Solid Electrolytes and Interface Formation Processes for Bulk-Type All-Solid-State Li and Na Batteries. Front. Energy Res. 4, 1–13 (2016).

[40]. Morimoto, H., Yamashita, H., Tatsumisago, M & Minami, T. Mechanochemical Synthesis of New Amorphous Materials of 60Li2S-40SiS2 with High Lithium Ion Conductivity. J. Am. Ceram. Soc. 82, 1352 (1999).

[41]. Kondo, S., Takada, K. & Yamamura, Y. New lithium ion conductors based on Li2S-SiS2 system. Solid State Ionics. 53-6, 1183 (1992).

[42]. Kanno, R. & Maruyama, M. Lithium ionic conductor thio-LISICON: the Li2S-GeS2-P2S5 system. J. Electrochem. Soc. 148, A742 (2001).

[43]. Kato, Y. et al. High-power all-solid-state batteries using sulfide superionic conductors. Nat. Energy 1, 16030 (2016).

[44]. Seino, Y., Ota, T., Takada, K., Hayashi, A. & Tatsumisago, M. 16,A sulphide lithium super ion conductor is superior to liquid ion conductors for use in rechargeable batteries. Energy Environ. Sci. 7, 627–631 (2014).

[45]. Tachez, M., Malugani, J. P., Mercier, R. & Robert, G. Ionic conductivity of and phase transition in lithium thiophosphate Li3PS4. Solid State Ionics 14, 181–185 (1984).

[46]. Muramatsu, H., Hayashi, A., Ohtomo, T., Hama, S. & Tatsumisago, M. Structural change of Li2S-P2S5 sulfide solid electrolytes in the atmosphere. Solid State Ionics 182, 116–119 (2011).

[47]. Hayashi, A., Muramatsu, H., Ohtomo, T., Hama, S. & Tatsumisago, M. Improved chemical stability and cyclability in Li2S-P 2S5-P2O5-ZnO composite electrolytes for all-solid-state rechargeable lithium batteries. J. Alloys Compd. 591, 247–250 (2014).

[48]. Luntz, A. C., Voss, J. & Reuter, K. Interfacial Challenges in Solid-State Li Ion Batteries. J. Phys. Chem. Lett. 6, 4599–4604 (2015).

[49]. Aurbach, D., Zinigrad, E., Cohen, Y. & Teller, H. A short review of failure mechanisms of lithium metal and lithiated graphite anodes in liquid electrolyte solutions. Solid State Ionics 148, 405–416 (2002).

[50]. Zeier, W. G. & Janek, J. A solid future for battery development. Nat. Energy 1, 16141 (2016).

[51]. Rabenau, A. Lithium nitride and related materials case study of the use of modern solid state research techniques. Solid State Ionics 6, 277–293 (1982).

[52]. Sakamoto, R., Tatsumisago, M & Minami, T. Preparation of Fast Lithium Ion Conducting Glasses in the System Li2S-SiS2-Li3N. J. Phys. Chem. B. 103, 4029-4031 (1999).

[53]. Bard, A. J. et al. ELECTROCHEMICAL METHODS Fundamentals and Applications. Electrochemistry. I. Faulkner, Larry R (1944). doi:10.1016/B978-0-12-381373-2.00056-9

[54]. Jiang, S. P., Love, J. G. & Badwal, S. P. S. Electrochemical Techniques in Studies of Solid Ionic Conductors. Key Eng. Mater. 125–126, 81–132 (1997).

[55]. University of Cambridge. Linear Sweep and Cyclic Voltametry: The Principles Title. Dep. Chem. Eng. Biotechnol. http://www.ceb.cam.ac.uk/research/groups/rg-eme/te (2015).

[56]. Evans, D. H., O'Connell, K. M., Petersen, R. A. & Kelly, M. J. Cyclic Voltammetry. 60, 290–293 (1983).

[57]. Lepley, N. D., Holzwarth, N. A. W. & Du, Y. A. Structures, Li+ mobilities, and interfacial properties of solid electrolytes Li3PS4 and Li3PO4 from first principles. Phys. Rev. B - Condens. Matter Mater. Phys. 88, 21–23 (2013).

[58]. Zhu, Y., He, X. & Mo, Y. Origin of Outstanding Stability in the Lithium Solid Electrolyte Materials: Insights from Thermodynamic Analyses Based on First-Principles Calculations. ACS Appl. Mater. Interfaces 7, 23685–23693 (2015).

List of Publications

Jie Yue, Fudong Han, Xiulin Fan, Xiangyang Zhu, Zhaohui Ma, Jian Yang and Chunsheng Wang . High-Performance All-Inorganic Solid-State Sodium-Sulfur Battery with a Na_3PS_4-Na_2S-Carbon Nanocomposite Cathode. (Submitted to ACS NANO on 2/28/2017 and is under review)